Absorptive effects in exclusive diffraction dissociation*

Edmond L. Berger and Pekka Pirilä
High Energy Physics Division, Argonne National Laboratory, Argonne, Illinois 60439
(Received 14 July 1975)

We report a detailed investigation of absorptive corrections in Good-Walker and Deck-type models for production of three-body final states in diffraction dissociation processes. Beginning with an input elastic diffractive amplitude which is central in impact parameter, the model generates naturally a peripheral structure for inelastic diffraction. For $pp \to (n\pi^+)p$ and $np \to (p\pi^-)p$, at small excitation mass, absorptive effects create significant dip structure in the production momentum transfer distribution $d\sigma/dtdM$ near $t \simeq -0.3$ $(\mathrm{GeV}/c)^2$, in agreement with data from Fermilab and the CERN ISR. Similar behavior is predicted for $\pi p \to A_1 p$ and $Kp \to Qp$, but at larger $|t|$. Distributions in other kinematic variables are much less affected by absorption. We provide a decomposition of the total $d\sigma/dtdM$ into partial cross sections for the various angular momentum and helicity states which comprise the low-mass diffractive enhancement. The s-wave amplitude is dominant in both absorbed and unabsorbed models. A pronounced mass-slope correlation is present both in the total $d\sigma/dtdM$ and in the s-wave part alone.

I. INTRODUCTION

The prominence of diffractive excitation in inelastic hadronic reactions is a striking experimental result with significant theoretical implications.[1] Although the processes were observed at conventional accelerators, it was only with the extended range of energy available at the CERN Intersecting Storage Rings (ISR) and at the Fermi National Accelerator Laboratory (Fermilab) that their diffractive nature could be verified unambiguously.[1] Several investigations at both laboratories are in progress aimed at establishing further properties, in both exclusive and inclusive reactions.

Exclusive diffractive processes with the lowest multiplicities are the easiest to examine in detail.[1-4] Among these we may list

$$pp \to p(n\pi^+), \tag{1a}$$

$$np \to (p\pi^-)p, \tag{1b}$$

$$pp \to p(p\pi^+\pi^-), \tag{1c}$$

and

$$\pi p \to (3\pi)p. \tag{1d}$$

The excited system is indicated in parentheses. The cross section is concentrated at relatively small mass M of this system,[2-4] $M < 2$ GeV, although the excitation spectrum may well extend to very high values. Resonances may be present in the data as well as a broad continuum. In analyzing such reactions as effective quasi-two-body processes, one usually defines a quasielastic differential cross section in terms of the momentum transfer t to the isolated proton. The cross section is confined sharply to small t values.

Notable constrasts are apparent when the (quasielastic) t dependence of $d\sigma/dtdM$ is compared with that of $d\sigma/dt$ for elastic scattering. In elastic scattering at ISR energies,[5] $d\sigma/dt$ falls in featureless, roughly exponential fashion by over six orders of magnitude from its maximum at $t=0$, before encountering a sharp minimum at $|t| \simeq 1.4$ $(\mathrm{GeV}/c)^2$. When recast in impact-parameter language, these data imply that diffractive *elastic* scattering is a central process,[5] concentrated about zero impact parameter. In contrast, in inelastic diffraction at small values of excitation mass, M, Fermilab data[3] on reaction (1b) and ISR data[2] on reaction (1a) show a dip or at least a break in $d\sigma/dtdM$ at $|t| \simeq 0.2$ $(\mathrm{GeV}/c)^2$ (after a precipitous fall from the maximum at $t=0$). A dip at such small $|t|$ implies peripheral structure in impact parameter,[6] with the cross section peaking at about 1 Fermi. Although a break near $|t| \simeq 0.2$ $(\mathrm{GeV}/c)^2$ has been observed in some lower-energy data,[7] below 30 GeV/c, the possibility existed that the effect was a nonasymptotic, nondiffractive phenomenon. The ISR and Fermilab results demonstrate the diffractive nature of the inelastic structure. They compel the conclusion that quasielastic scattering is peripheral in impact parameter, whereas elastic scattering is central.

The Deck model[8] has been used extensively to interpret the production and decay characteristics of nonresonant low-mass enhancements in the (πa^*) system in diffraction dissociation reactions of the type

$$ap \to (a^*\pi)p. \tag{1e}$$

Here, a is an incident hadron from the set $K^\pm$, $\pi^\pm$, K^0, $\bar{K}^0$, p, $\bar{p}$, n, and so forth. The model has enjoyed a considerable measure of at least qualitative success,[8] although difficulties become apparent in detailed experimental comparisons.[8] In

particular, according to the model, the distribution in momentum transfer to the diffractively scattered proton should resemble that for elastic scattering, thus showing no structure at $|t| \simeq 0.2$ $(\mathrm{GeV}/c)^2$ in reactions (1a) and (1b). A related problem concerns the variation with mass M of the small t slope of $d\sigma/dtdM$. A marked decrease of slope is observed in the data as mass M is increased above the threshold value $(m_\pi + m_{a^*})$. While explained qualitatively by the model, this "mass-slope" correlation has not been satisfactorily reproduced quantitatively in calculations to date.[9]

In addition to these difficulties in practice, there are questions of principle which lead one to reexamine the model. In inelastic two-body and quasi-two body reactions, absorptive corrections[10] are found to be often important. Such effects should *a priori* be included also in a proper calculation of two- to three-body reactions of type (1). The role, indeed, necessity of such absorption terms is further apparent when one adopts the optical interpretation of diffraction dissociation.[11]

In this article we report a detailed investigation of absorption corrections to Deck-type models of diffraction dissociation. Our approach is similar in spirit to that of Tsarev,[12] although we differ in choice of absorption terms and in quantitative results. We begin in Sec. II with a discussion of which single- and double- (absorptive) scattering amplitudes are important. Arguments based on both the optical approach and the double-peripheral model lead to similar conclusions. Adopting a simple exponential parametrization of the single-scattering terms, we show in Sec. III that the loop integrals involved in obtaining the absorptive corrections can be evaluated analytically. The resulting absorbed diffraction dissociation amplitudes are used to compute various mass, momentum transfer, and angular distributions. We also present a partial-wave decomposition of our amplitudes.

We show that absorption of the expected strength produces significant structure in the momentum transfer distributions, similar to that observed in the data from reactions (1a) and (1b). In particular, our differential cross sections $d\sigma/dtdM$ show a pronounced break, whose position moves to larger $|t|$ as M increases. We analyze our low-mass enhancement into the contributions from the different spin and helicity (L, λ) states of which it is composed. An examination of the partial differential cross sections $d\sigma^{L\lambda}/dMdt$ shows that for each component, the dip location is not fixed in $|t|$, but moves to larger $|t|$ as M increases. This explicit result is in contrast to assumptions made in some models[13] based on "universality in impact-parameter space." In our approach, the mass-slope correlation is present in the dominant $(L=0, \lambda=0)$ partial cross section, as well as in the total.

In addition to its dramatic influence on the t distribution itself, absorption accentuates the mass-slope correlation and provides good agreement with experimental determinations of the slope. When we compare other distributions integrated over t (e.g., mass, decay angles), we find little difference between our absorbed and nonabsorbed results.

In Sec. IV we drop the exponential parametrization and study more realistic models for momentum transfer dependences. Dropping the exponential parametrization results in somewhat more complicated expressions, which can nevertheless be evaluated numerically. We treat amplitudes appropriate to the experimental situations $NN \to (N\pi)N$ in Sec. IV B and $\pi p \to (\rho\pi)p$ or $Kp \to (K^*\pi)p$ in Sec. IV C. Detailed results are presented. There are no undetermined parameters in our approach. The agreement we achieve with data supports the Deck interpretation of diffractive threshold enhancements, as well as the necessity for absorptive corrections to the model.

In Sec. V we summarize our conclusions, and we comment briefly on polarization and cross-over predictions in the absorbed Deck model.

II. MODEL FOR DIFFRACTIVE DISSOCIATION

In this section we develop heuristic arguments to justify the set of single- and double-scattering graphs which we employ. We present two different methods of reasoning, which lead to essentially the same conclusions. First, we discuss the single-scattering terms (II A) and then the absorptive corrections (II B). Appendixes A and B supplement the material of these subsections. In Sec. II C we give an explicit integral expression for the absorbed Deck amplitude.

A. Single-scattering terms

As a direct generalization of exchange dynamics appropriate in two-body reactions, one may expect that two- to three-body processes are described by a set of double-peripheral graphs typified by Fig. 1(b), where R_1 and R_2 denote allowed exchanges. This graph would be expected to be dominant in the kinematic region defined by "small" t_1 and t_2, as well as "large" s_1 and s_2. Our interest is in the high-energy double-peripheral description of the diffractive reaction (1e), at small values of the (πa^*) mass and small momentum transfer t_1. Because the (πa^*) mass is small, we

should expect, *in the context of an exchange model description,* that there will be significant effects in the data attributable to both the "t-channel" and "u-channel" graphs drawn in Figs. 2(a) and 2(b). Indeed, experimental checks show that characteristics of both are present, in roughly equal weight.[8] This is not to imply, however, that one has learned how to properly add amplitudes corresponding to t- and u-channel exchange effects. A third graph may also contribute, although its role is highly ambiguous. This graph is sketched in Fig. 2(c).

An argument to suggest that all three graphs may play a role in hadronic production was made by Fox.[14] Closing one's eyes to the profound differences between the Pomeron (whatever it is) and the photon, one can quickly convince oneself that if the wavy lines in Fig. 2 were photon lines, and all hadrons were elementary particles, then all three graphs would have to be computed. Moreover, their sum vanishes at $t_1 = 0$. Surely this analogy is at best qualitatively instructive, and in the realistic hadronic situation the weights of the three graphs are not determined easily.

In Appendix A we develop the semiclassical optical approach[11] to diffraction dissociation. This approach is very different in conception from the double-peripheral model discussed just above. However, it is gratifying that the two methods lead to the same set of three single-scattering graphs, sketched in Fig. 2.

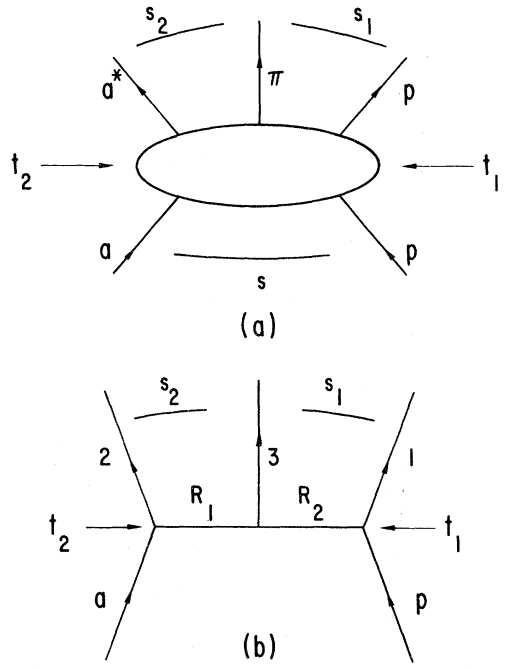

FIG. 1. (a) Diagram illustrating the independent Lorentz-invariant kinematic variables for $ap \to a^*\pi p$. (b) Double-peripheral exchange graph for $ap \to 123$. Symbols R_1 and R_2 denote exchanges.

The parametrization of the pion-exchange graph, Fig. 2(a), is relatively unambiguous, because the π is not far off the mass shell (Sec. IV). Treatment of the "u-channel" a^*-exchange graph is less clean, but its qualitative effects are clear.[8] The third graph, with a direct channel, off-shell scattering of particle a, is an enigma. Its role is uncertain from a duality point of view and, as of yet, no direct evidence for or against the effects of graph (c) has been identified in data. For these reasons, we will not treat it quantitatively in this article. However, we note here that the $(a^*\pi)$ system produced by this graph (c) has the same spin, parity, and s-channel helicity as the initial state a. For $\pi p \to (\rho\pi)p$ and $Kp \to (K^*\pi)p$, therefore, graph (c) provides $J^P = 0^-(\rho\pi)$ and $(K^*\pi)$ enhancements, respectively, whereas graphs (a) and (b) provide predominantly $J^P = 1^+$ waves (Sec. IV). The Illinois group[15] made a detailed comparison of partial-wave decompositions of the π-exchange Deck amplitude and data. They found that the pion-exchange Deck graph is in substantial agreement with data, save that there is a factor of 2 too much 0^- cross section in the model. Graph (c), with the negative sign suggested by the optical model, would remedy this discrepancy nicely.

Before turning to absorptive corrections, we remark that the three graphs in Fig. 2 are to be understood as nonresonant "background" graphs. Identified resonances are present in several diffractive reactions [e.g., A_2 in $\pi p \to (\rho\pi)p$ and K^*_{1420} in $Kp \to (K^*\pi)p$]. We do not treat these resonant contributions. Moreover, there may be other resonances not yet disentangled from the (πa^*) low-mass background enhancement. Indeed the search for the $J^P = 1^+ A_1$ and Q resonances remains an important experimental pursuit.[8]

B. Absorptive corrections

Ignoring graphs which correspond to vertex corrections, we may identify a considerable number of second scattering absorptive amplitudes. These

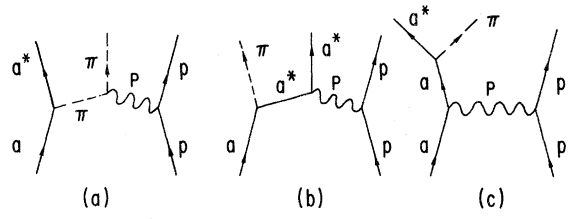

FIG. 2. The three pole terms for the diffractive process $ap \to a^*\pi p$. The wavy line labeled P denotes elastic scattering. (a) The "t-channel" pion-exchange pole graph; (b) the "u-channel" a^*-exchange pole graph; (c) the direct "s-channel" graph.

are drawn in Fig. 3 for the pion-exchange single-scattering term of Fig. 2(a). The wavy lines in all instances represent diffractive scattering of the two particles joined by the line. A similar set is associated with Figs. 2(b) and 2(c). As described in Appendix A, in the optical approach to diffraction dissociation, *only the graphs (c) and (d) of Fig. 3 are instrumental.* The others do not contribute. The same conclusion may be reached in the context of the double-peripheral approach, as we will now show. Readers not interested in this rather long but necessary discussion may skip to Sec. IIC.

We begin by classifying the graphs in Fig. 3 into four sets. Graphs (a) and (b) are termed "initial-state" absorption. They involve the elastic scattering of the *incident* particles a and p. As demonstrated by a detailed technical argument in Appendix B, these graphs do not contribute significantly at high energy. The essential physical reason for this is that the dissociation $a \to a^*\pi$ occurs in the center-of-mass frame a long time before the system $(a^*\pi)$ interacts with the target proton. [The lifetime of the $(a^*\pi)$ state is proportional to $\gamma = E_a/M_a$.] Graphs (c) and (d) are the "final-state" absorption corrections. Together they provide the dominant absorptive effect and are discussed in detail below. Graphs (e)–(h) are absorptions associated with the pion-exchange line. Because the subenergy s_2 is not far above

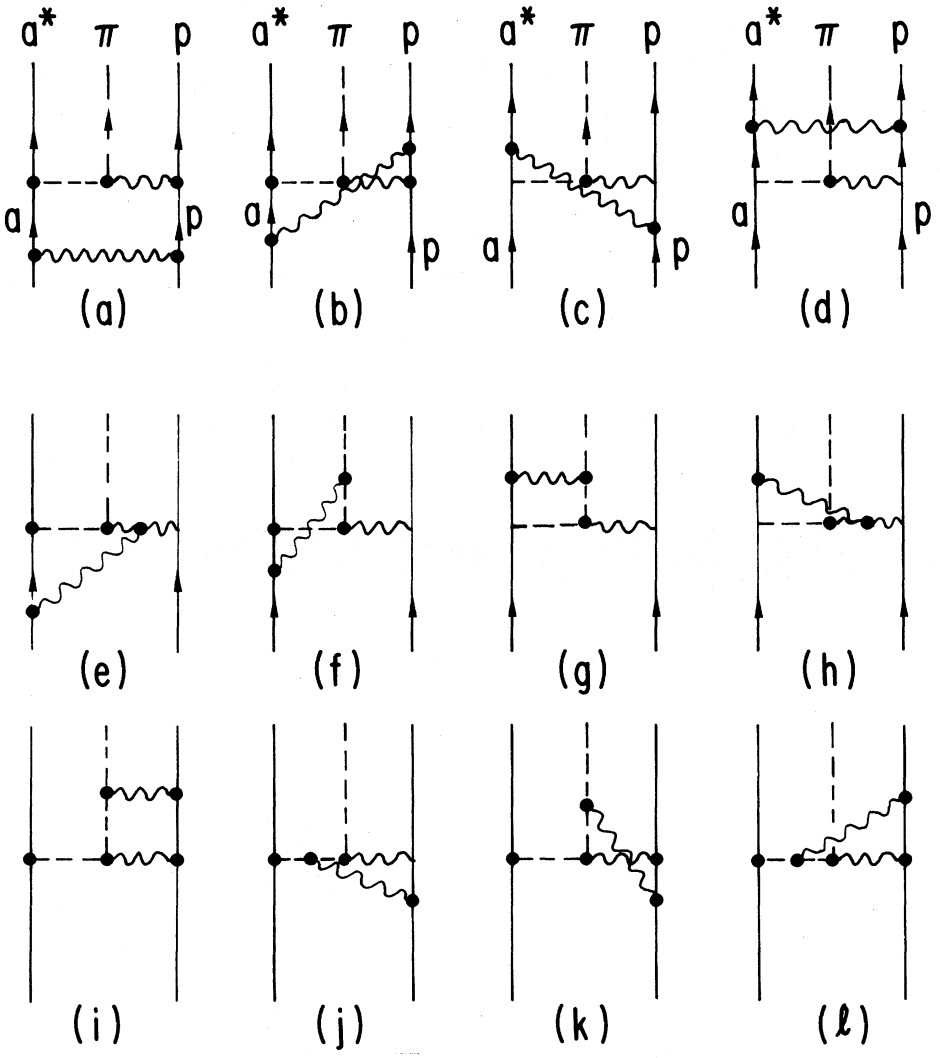

FIG. 3. The 12 lowest-order absorptive correction terms for the "t-channel" pion-exchange Deck graph. All wavy lines denote elastic scattering.

threshold, it is unclear what these terms signify. In any case, absorption of the π (or a^*) is best handled by the traditional (although not compelling) techniques of two-body scattering. An investigation of such corrections to the pion-exchange Deck graph was reported by Berger and Irving.[16] The conclusion is that absorption of the pion (in this sense) does not significantly modify properties of the unabsorbed amplitude. We will assume henceforth that in the parametrization of the amplitudes we use, standard two-body t-dependent effects associated with absorption of the pion are effectively included.

The fourth set of second scattering terms, Figs. 3(i)–3(l), represents elastic absorption of the $\pi_{\text{off}}p \to \pi p$ amplitude. However, as is customary in practical applications of the model,[8] we interpret our Deck amplitudes as already incorporating the full (off-shell) elastic scattering amplitude, Therefore, these four terms are effectively included in our parametrization of the single-scattering graphs.

Having disposed of most of the graphs in Fig. 3, we now turn to an analysis of the important two graphs, Figs. 3(c) and 3(d). If we employ elementary particle propagators in the intermediate state of the "box diagrams" drawn in Fig. 3, the same argument (cf. Appendix B) which led to suppression of graphs (a) and (b) permits us to use on-shell propagators for the particles a^* in graphs (c) and (d). Moreover, the sum of the amplitudes for graphs (c) and (d) contains the full on-shell propagator for the intermediate-state proton. The off-shell parts cancel. The sum is then well represented numerically by either graph (c) or (d), with the full on-shell part of the propagator for p. These last statements are true to the extent that the ratio $(M_{a^*\pi}/\sqrt{s})$ is a small parameter. Since our interest is restricted to values of $M_{a^*\pi}$ just above threshold, the requirement is satisfied.

We admit that the above arguments lack fundamental rigor and are subject to doubts similar to those raised concerning the absorption approach in general.[10]

C. Variables and parametrizations

The amplitude for a two- to three-particle reaction A_0 depends in general on five independent kinematic variables. Our set (s, s_1, s_2, t_1, t_2) is indicated in Fig. 1(a). The elastic scattering amplitude A_{el} depends on two variables, an appropriate s and t. We use primed quantities for intermediate-state variables, which are integrated over. Following the discussion at the end of the preceding section, we express the absorptive amplitude corresponding to Fig. 3(d) as

$$A_{\text{abs}} = i \int \frac{d^4q_3}{(2\pi)^4} A_{\text{el}}^{a^*p}(s_{12}, t_3) A_0(s, t_1', t_2', s_1', s_2') \times 2\pi\delta(p_2'^2 - m_{a^*}^2) 2\pi\delta(p_1'^2 - m_p^2). \quad (2)$$

Variables are defined according to Fig. 4. Four-vector momentum is conserved at each vertex.

$$s_{12} = (p_1 + p_2)^2.$$

Another expression may in principle be written for Fig. 3(c). However, it differs from Eq. (2) only in terms which are of order $(M_{a^*\pi}/\sqrt{s})$ and, moreover, as remarked above, the use of the on-shell propagator is justified only for the sum of the two amplitudes. Thus, Eq. (2) serves as our full absorption term.

After some uninspiring algebra and integrating to remove the two delta functions, consistently dropping correction terms of order $(M_{a^*\pi}/\sqrt{s})$, we obtain

$$A_{\text{abs}} = \frac{i}{8\pi^2 s_{12}} \int d^2\vec{q}_{3T} A_{\text{el}}^{a^*p}(s_{12}, t_3) A_0(s, t_1', t_2', s_1', s_2'), \quad (3)$$

with

$$t_3 = -\vec{q}_{3T}^{\,2}, \quad (4)$$

$$t_1' = t_1 - (\vec{q}_{3T}^{\,2} + 2\vec{q}_{3T} \cdot \vec{p}_{1T}), \quad (5)$$

$$t_2' = t_2 - \frac{1}{\chi_2}(\vec{q}_{3T}^{\,2} - 2\vec{q}_{3T} \cdot \vec{p}_{2T}), \quad (6)$$

$$\chi_2 = p_{2L}/p_{CM} = 2p_{2L}/\sqrt{s}, \quad (7)$$

$$s_1' = s_1 + \vec{q}_{3T}^{\,2}\left(1 - \frac{1}{\chi_2}\right) + 2\vec{q}_{3T} \cdot \left(\vec{p}_{1T} + \frac{1}{\chi_2}\vec{p}_{2T}\right). \quad (8)$$

The two-dimensional transverse vectors $\vec{p}_{1T}$ and $\vec{p}_{2T}$ are the transverse components of the momenta of final-state particles p and a^*, respectively; p_{2L} is the center-of-mass longitudinal component of a^*. Equation (3) is rather general. To make

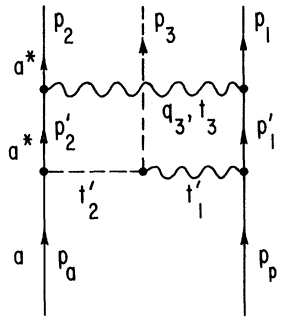

FIG. 4. Diagram illustrating the kinematic variables for the absorptive graph of Fig. 3(d).

further progress, we must adopt specific parametrizations of the Deck and elastic amplitudes. These issues are taken up in Secs. III and IV.

III. EXPONENTIAL PARAMETRIZATION OF AMPLITUDES

A. General analysis

A conventional asymptotic exponential parametrization of elastic scattering, which we adopt also, is

$$A_{el}^{ab}(s,t) = is\sigma^{ab}\exp(B_3 t), \tag{9}$$

where σ^{ab} stands for the ab total cross section. For the moment, secondary Regge terms of order $s^{1/2}$ are ignored; we comment on their role below.

The essential kinematic ingredients of either the π-exchange or the a^*-exchange Deck amplitudes [Figs. 2(a) and 2(b)], which lead to a strong enhancement of the cross section near threshold in the $(a^*\pi)$ subenergy, are expressed simply as[8]

$$A_\pi(s_{\pi p}, t_{aa^*}, t_{pp}) = ig_\pi(t_{aa^*})\sigma^{\pi p}s_{\pi p}\exp(B_\pi t_{pp}) \tag{10}$$

and

$$A_{a^*} = ig_{a^*}(t_{a\pi})\sigma^{a^* p}s_{a^* p}\exp(B_{a^*}t_{pp}). \tag{11}$$

The functions g_π and g_{a^*}, which stand for the particle propagators, decrease in magnitude as their respective $(-t_i)$ increase. The factor $is_{\pi p}\sigma^{\pi p}\exp(B_\pi t_{pp})$ represents the essential structure of the (off-shell) πp diffractive elastic scattering, likewise for $is_{a^* p}\sigma^{a^* p}\exp(B_{a^*}t_{pp})$. More sophisticated parametrizations for the elastic amplitude (including rotating phase Regge terms) easily come to mind. Reggeization of the π and a^* improves fits to data,[8] while also increasing the complexity of Eqs. (10) and (11). In this section we adopt the simplest stripped-down parametrization of the single-scattering terms. We set

$$g_\pi(t_{aa^*}) = \exp(B_2 t_{aa^*}). \tag{12}$$

As a result, we are able to evaluate explicitly the integrals in Eq. (3). Since these simplified expressions contain the kinematic essence of more complete formulas, we gain in analytic understanding while sacrificing little. In Sec. IV we examine results in which

$$g_\pi = (-t_{aa^*})^{1/2}\exp(t_{aa^*})/(m_\pi^2 - t_{aa^*}) \tag{13}$$

and

$$g_\pi = (m_\pi^2 - t_{aa^*})^{-1}. \tag{14}$$

Inserting Eqs. (9), (10), and (12) into Eq. (3), we obtain

$$A_{abs} = -A_0(s_1, t_2, t_1)\frac{\sigma^{a^* p}}{8\pi B} \times\exp\left[\frac{1}{B}\left(B_1\vec{p}_{1T} - \frac{1}{|\chi_2|}B_2\vec{p}_{2T}\right)^2\right], \tag{15}$$

with

$$B = B_1 + \frac{1}{|\chi_2|}B_2 + B_3. \tag{16}$$

The unabsorbed Deck amplitude, which appears in Eq. (15) as a factor, is

$$A_0(s_1, t_2, t_1) = i\sigma^{\pi p}s_1\exp(B_1 t_1 + B_2 t_2). \tag{17}$$

The full scattering amplitude is

$$A = A_0 + A_{abs}. \tag{18}$$

In interpreting Eq. (15), it is useful to notice that to leading order in s, the momentum transfer t_1 and t_2 are given by ($|\chi_1| = 1$)

$$t_1 = -\vec{p}_{1T}^{\,2}, \tag{19}$$

$$t_2 = -\frac{1}{|\chi_2|}\vec{p}_{2T}^{\,2} + m_a^2(1 - |\chi_2|) + m_{a^*}^2(1 - 1/|\chi_2|). \tag{20}$$

Therefore, the exponential factor in Eq. (15) is an increasing function of $(-t_1)$ and $(-t_2)$. We observe directly the expected result that the double-scattering or absorption amplitude has a weaker dependence on t_1 and t_2 than the unabsorbed amplitude. Since the two amplitudes differ in sign, one expects cancellation to occur and, therefore, a zero of the full amplitude A, at some well-defined values of t_1 and t_2.

B. Structure in momentum transfer t_1

The most dramatic effect of absorption is observed in the momentum transfer distribution $d\sigma/dt_1$ for production of the low-mass diffractive enhancement. This result can be seen directly from Eqs. (15)–(18). At the threshold $M_{a^*\pi} = (m_{a^*} + m_\pi)$,

$$\vec{p}_2 = \frac{m_{a^*}}{(m_{a^*} + m_\pi)}\vec{p}_{a^*\pi}, \tag{21}$$

where $\vec{p}_{a^*\pi}$ $(= -\vec{p}_1)$ is the momentum of the $(a^*\pi)$ system. Therefore,

$$\vec{p}_{2T} = -|\chi_2|\vec{p}_{1T}, \tag{22}$$

and the exponential factor in Eq. (15) becomes $\exp[-(1/B)(B_1 + B_2)^2 t_1]$. Consequently, *the full amplitude*, Eq. (18), *passes through zero* at

$$t_1^{(0)} = \frac{-B}{(B_1 + B_2)^2}\ln\left(\frac{8\pi B}{\sigma^{a^* p}}\right). \tag{23}$$

We now select the specific dissociation process $pp \to p(n\pi^+)$ at 100 GeV/c in order to specify parameters and determine the value of $t_1^{(0)}$. For small values of $M_{n\pi^+}$, the typical value of $\sqrt{s_1}$ is $\sqrt{s}/2$ and $s_{12} \simeq s$. Thus, the elastic scattering parameters $B_1 = 4.5$ (GeV/c)$^{-2}$ and $B_3 = 5.5$ (GeV/c)$^{-2}$ are reasonable, with $\sigma^{np} \simeq 38$ mb $= 98$ GeV^{-2}. An

exponential is not a very decent approximation to the pion-exchange t dependence of $(-t_2)^{1/2}\exp(t_2 - m_\pi^2)/(m_\pi^2 - t_2)$ (cf. Sec. IV). However, at the typical $\sqrt{s_1} \simeq \sqrt{s}/2$, an exponential form with $B_2 = 3$ $(\mathrm{GeV}/c)^{-2}$ does adequately over a reasonable t_2 interval. With these values we find

$$t_1^{(0)} \simeq -0.3 \ (\mathrm{GeV}/c)^2 . \tag{24}$$

A similar result was obtained by Tsarev.[12] Experimentally there is evidence for a dip or, at least, break in the distribution $d\sigma/dt_1$ when the mass $M_{n\pi^+}$ is near threshold. The position of this structure in the data[2,3] is close to -0.2 $(\mathrm{GeV}/c)^2$. The zero we obtain is at somewhat too large $|t_1|$, indicating that the absorption term (at $M_{n\pi^+}$ threshold) is perhaps too weak.

At values of $M_{a*\pi}$ above its threshold, the equality given by Eq. (22) no longer holds, and one must integrate over allowed values of $\vec{p}_{2T}$. The result is that the predicted dip in $d\sigma/dt_1$ disappears gradually as $M_{a*\pi}$ is increased. This is illustrated in Fig. 5. Owing to this variation of dip location with mass, essentially no structure in t is expected in $d\sigma/dtdM$ if a relatively large interval (e.g., $\Delta M \gtrsim 0.5$ GeV) in M is averaged or integrated over, as is often the case in bubble-chamber analyses, or in experiments with poor mass resolution.

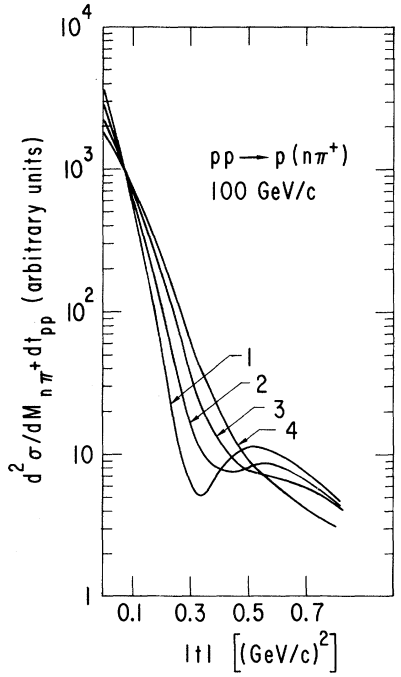

FIG. 5. Double-differential cross section $d^2\sigma/dM_{n\pi^+}dt_{pp}$ for $pp \to pn\pi^+$ at 100 GeV/c averaged over four intervals of mass: (1) $M_{n\pi^+} \leq 1.2$ GeV; (2) $1.2 \leq M_{n\pi^+} \leq 1.3$ GeV; (3) $1.3 \leq M_{n\pi^+} \leq 1.4$ GeV; (4) $1.4 \leq M_{n\pi^+} \leq 1.5$ GeV. All curves are normalized to give the same value when integrated over t_{pp}. These curves are obtained from the exponential model of Sec. III.

Because meson-nucleon total cross sections are smaller than σ^{pp}, we expect absorptive effects to be less important in diffractive reactions induced by a meson beam, e.g., $\pi p \to A_{1p} \to (\rho\pi)p$, $Kp \to Qp \to (K^*\pi)p$, and $\pi p \to \pi(N\pi)$. The position of the dip or break in $d\sigma/dt_1$ moves out to larger $|t_1|$, as shown explicitly in Sec. IV C.

It is useful to recast the results of the above paragraphs in impact-parameter language. The elastic-scattering amplitude and the *unabsorbed* π-exchange Deck amplitude have roughly exponential dependence on momentum transfer t_3 and t_1', respectively [cf. Eqs. (9) and (17)]. Therefore, both are approximately Gaussian functions of impact parameter, and represent *"central"* collisions. Absorption generates a zero at $t_1 \simeq -0.3$ $(\mathrm{GeV}/c)^2$, as discussed. When translated to impact space, this means that the central partial waves are depleted. At small values of the mass of the excited system, the resulting diffractive inelastic *absorbed* Deck amplitude has a peripheral impact-parameter structure.

The parametrization for elastic scattering which we adopted in Eq. (9) is equivalent to describing the process by a fixed pole Pomeron ($\alpha_p = 1 + \alpha' t$ with $\alpha' = 0$). This means that we abandon from the start any pretention to "predict" a logarithmic (or other) energy variation for the position of the dip in $d\sigma/dt_1$. On the other hand, the parameters selected to describe the t dependence of elastic scattering are taken from the data. Therefore, B_1 and B_3 in Eqs. (16) and (23) increase linearly with $\ln s$, implying that $|t_1^{(0)}|$ should decrease as $(\ln s)^{-1}$.

C. Other effects of absorption

In the preceding subsection we stressed the most dramatic effect of absorption. It increases the slope of the production differential cross section $d\sigma/dt_1 dM$ at small t_1 and produces a mass-dependent dip/break structure near $|t_1| = 0.3$ $(\mathrm{GeV}/c)^2$. Other properties may also be recognized by inspection of the simple Eq. (15). We collect a few of these general observations here, leaving quantitative details to Sec. IV. Readers interested primarily in results of immediate relevance to data are advised on first reading to skip directly to Sec. IV.

1. Integrated cross sections

Because of the cancellation which occurs in Eq. (18), absorption obviously reduces the integrated cross section. In $pp \to p(n\pi^+)$, the reduction is roughly by one-half. Since absorption is somewhat weaker in $\pi p \to A_1 p$ and $Kp \to Qp$, the reduc-

tion is less. In practical comparisons with data,[8] the unabsorbed π-exchange Deck amplitude is variously found to yield between 0.3 and 1.5 of the experimental cross section. More cross section would be obtained if the contribution of the unabsorbed "u-channel" graph [e.g., K^* for $Kp \to Q^*p$, n for $pp \to p(n\pi^+)$] would be added to the t-channel π-exchange graph. Properties of these "u-channel" terms are observed in the data,[8] and, by use of the ϕ_s selection procedure described in Refs. 8 and 17, their integrated contribution can be estimated. Results for the ratio σ_{a*}/σ_π lie in the range $\frac{1}{3}$ to 1. Because the exchanges are relatively far off the mass shell, procedures for parametrizing the u-channel amplitudes are inherently uncertain. The addition of t- and u-channel exchange amplitudes or cross sections is also fraught with ambiguity. For these reasons we do not explicitly treat the u-channel contribution of Fig. 2(b) in this article. Our detailed analysis is reserved to the π-exchange (or t-channel) amplitude Fig. 2(a) and its absorptive corrections.

Contributions from the "u-channel" graphs could well offset the loss of cross section resulting from absorption, so that we do not consider the absorptive reduction a serious liability. The t-channel π and u-channel a^*-exchange amplitudes both yield a predominantly s-wave threshold enhancement and have similar dependences on the variable t_1. Therefore, our neglect of the a^*-exchange graph should not compromise the major conclusions of our study.

2. Mass slope correlation

At least two distinctive features characterize the mass-dependent behavior of the slope of the production differential cross section $d\sigma/dt_1$ for several high-energy exclusive inelastic hadronic processes of the type $ab \to 1(23)$. First, when the mass M_{23} of the (23) pair is near its threshold value (m_2+m_3), *the slope is particularly large* (as much as twice the slope of elastic scattering at the same beam momentum). Second, *the value of the slope falls rapidly* as M_{23} is increased above the threshold. Crudely, a factor of 2 drop in slope over an M_{23} mass interval of 0.5 GeV above threshold is followed by a rather gradual decrease, or even rough constancy. This pronounced *mass-slope correlation near threshold* has been recognized for some years[8,9] in data from exclusive reactions of the diffraction dissociation class, for example in $Kp \to (K\pi\pi)p$, $\pi p \to (3\pi)p$, and $pp \to (N\pi)p$.

In the *unabsorbed* Deck model, this near-threshold mass-slope correlation emerges naturally.[8] It is a consequence of the double-peripheral structure in the momentum transfer of the graphs in Figs. 2(a) and 2(b). Indeed, near threshold, the momentum transfer t_1 and t_2 are linearly related,[8]

$$t_2 = \frac{(m_{a*}t_1 + m_\pi m_a^2)}{(m_{a*}+m_\pi)} - m_{a*}m_\pi . \tag{25}$$

Substituting Eq. (25) in Eq. (17), we find that the dependence on t_1 of the unabsorbed Deck amplitude near threshold becomes

$$A_0 \propto \exp\left\{\left[B_1 + B_2\left(\frac{m_{a*}}{m_{a*}+m_\pi}\right)\right]t_1\right\} . \tag{26}$$

Using the parameters quoted in Section III B, we obtain $A_0 \propto \exp(7.1t_1)$, to be compared to the elastic $A_{el} \propto \exp(4.5t_1)$ at the same energy. At large $(M_{a*\pi})$, the constraint no longer holds and

$$A_0 \propto \exp(4.5t_1) . \tag{27}$$

The net effect yields a slope of $d\sigma/dt_1$ which is particularly large near the threshold in $M_{a*\pi}$. The slope then decreases rapidly as $M_{a*\pi}$ is increased. The result derives from the structure of A_0 in the t variables. No assumptions are necessary concerning dependence on subenergy variables.

Absorptive effects enhance the mass-slope correlation by sharpening the distribution $d\sigma/dt_1$ near threshold. It was demonstrated above that absorption provides a zero in $d^2\sigma/dt_1 dM_{a*\pi}$ at $t_1 \simeq -0.3$ $(\mathrm{GeV}/c)^2$ when $M_{n\pi^+} = (m_n + m_\pi)$. Numerical calculations show that the zero of the amplitude moves slowly to larger $|t_1|$ with increasing $M_{n\pi}$. Because the location of the zero depends also on the other two kinematic variables (t_2 and $s_{\pi p}$), the dip in $d^2\sigma/dt_1 dM_{n\pi}$ gradually transforms into a break (by $M_{n\pi} = 1.3$ GeV), Fig. 5. It disappears altogether at higher $M_{n\pi}$. Correspondingly, the slope of $d\sigma/dt_1$ in the small t region $0 \leq |t_1| \leq 0.2$ $(\mathrm{GeV}/c)^2$ changes from roughly 20 $(\mathrm{GeV}/c)^{-2}$ at threshold to 10 $(\mathrm{GeV}/c)^2$ at $M_{n\pi} = 1.5$ GeV, in this example. The value 20 is to be compared to 14 for the unabsorbed model. Comparisons in Sec. IV show that the absorbed calculation is in much better agreement with data.

As described above, the mass-slope correlation arises in the pion-exchange Deck model from a convolution of momentum transfer dependences. This is true also of the absorbed model. The mechanism can be tested by analyzing the data in the full four-dimensional space.[9] In the model this effectively removes the convolution effect and the mass-slope correlation disappears.

It has been found that the variation of slope with mass in the data is essentially the same for the two methods. Thus, the model explanation is at best incomplete. It works for $d\sigma/dt_1 dM$, but it fails in the four-dimensional analysis. Absorption does not remedy the problem. As far as we can determine, no model in the literature has been

shown to survive the four-dimensional test. We believe that the mass-slope correlation effect in the full four-dimensional space can be obtained properly only after both the u-channel and t-channel graphs, Figs. 2(a) and 2(b), are included in the calculation. Preliminary analyses verify this conjecture. We expect to report the results elsewhere.

3. Structure and properties of the low-mass enhancement

Although absorption produces mass-dependent structure in the production momentum transfer distribution $d\sigma/dt_1$ and reduces the integrated cross section, it modifies the shape $d\sigma/dM_{a*\pi}$ of the low-mass diffractive enhancement very little. Absorption appears not to yield the sharpening effect which might be desirable in improving fits to data.[8]

The Deck model predicts that the low-mass diffractive enhancement is predominantly in an orbital angular momentum $L=0$ state, in substantial agreement with data.[15] Other waves and nonzero helicity states are also present. The Deck amplitude for the process $ap \to a^*\pi p$ specifies the relative contributions of these partial amplitudes. We may decompose the amplitude A_0 as

$$A_0(s, s_2, t_1, s_1, t_2) = \sum_{L,\lambda} \mathcal{C}_{L,\lambda}(s, s_2, t_1) Y_{L,\lambda}(\theta, \phi). \tag{28}$$

Here (θ, ϕ) are decay angles in the $s_2 = M_{a*\pi}{}^2$ rest system, and L, λ are orbital angular momentum and helicity, respectively. We may work with either s-channel angles and helicities $(\theta_s, \phi_s, \lambda_s)$ or t-channel quantities $(\theta_t, \phi_t, \lambda_t)$. For the s-channel, the quantization axis is the direction of the final-state nucleon p, whereas for the t-channel, the axis is the direction of incident hadron a. In both cases, the production plane normal is $\vec{a}\times\vec{p}$. In Eq. (28) the five independent kinematic variables are (s, s_2, t_1, ϕ, and θ). The invariants s_1 and t_2 may be reexpressed simply in terms of these five, by use of formulas found, for example, in Ref. 8. We remark that in the present discussion we are implicitly treating all hadrons in $ap \to a^*\pi p$ as spinless. Spins and helicities (L, λ) refer only to the orbital angular momentum of the $(a^*\pi)$ system. Thus, appropriate care must be taken in translating our comments to the experimental situation.

Corresponding to partial-wave analysis of Eq. (28), we obtain the decomposition

$$\frac{d\sigma}{dt_1 dM} = \sum_{L,\lambda} \frac{d\sigma^{L,\lambda}}{dt_1 dM}. \tag{29}$$

It is interesting to examine the t_1 and M structure of each $\sigma^{L,\lambda}$, for both the absorbed and unabsorbed models. We do this explicitly in Secs. IV. Here we confine ourselves to a few general remarks. Because absorptive effects are greatest for states with s-channel helicity $\lambda_s = 0$ absorption increases the ratio $\sigma^{\lambda_s>0}/\sigma^{\lambda_s=0}$. However, since the $L=0$, partial cross section is so dominant, both before and after absorption, we observe little change in the $(a^*\pi)$ decay angular distributions $d\sigma/d\cos\theta$ and $d\sigma/d\phi$ themselves. This last remark is true for distributions integrated over all t_1, or for distributions restricted to small $|t_1|$. If one chooses a value of $|t_1|$ at which the absorbed $L=0$ wave vansihes ($t_1 \simeq -0.3$ (GeV/c)^2), the remark is obviously not correct. The detailed analysis of Sec. IV may be consulted regarding expectations for the t_1 dependence of the various L and λ components of the diffractive enhancement.

One significant conclusion of this study is that the strong mass-slope correlation is present in the dominant $L=0$ partial wave, by itself, in both the absorbed and unabsorbed amplitudes.

4. Nonasymptotic terms

The full diffraction dissociation amplitude $A_0 + A_{\rm abs}$ is

$$A = A_0 + A_{\rm el} \otimes A_0. \tag{30}$$

Here we have replaced the convolution integral Eq. (3) by the symbolic expression $A_{\rm el} \otimes A_0$. Decomposing $A_{\rm el}$ into terms with different dependence on energy, we may express it as

$$A_{\rm el}(s_{12}, t_3) = A_P + A_{R_1} + A_{R_2} + \cdots, \tag{31}$$

where $A_P \propto s_{12}$, $A_R \propto s_{12}{}^{\alpha_R}$, $\alpha_{R1} \simeq 0.5 + t_3$, and $\alpha_{R2} \simeq 0.0 + t_3$. Similarly, the Deck amplitude may be written as a series of terms with different dependence on the πN *subenergy*

$$A_0 = A_{0,P} + A_{0,R_1} + A_{0,R_2} + \cdots, \tag{32}$$

where

$$A_{0,P} \propto s'_{13}, \tag{33}$$

$$A_{0,R} \propto (s'_{13})^{\alpha_R}. \tag{34}$$

Upon substituting into Eq. (30), we obtain

$$A = [A_{0,P} + A_P \otimes A_{0,P}] + [A_{0,R_1} + A_{R_1} \otimes A_{0,P} + A_P \otimes A_{0,R_1}] + \cdots. \tag{35}$$

The forms chosen for the energy dependences of $A_{\rm el}$ and A_0 in Sec. III A resulted in our retaining only the first term in square brackets of Eq. (35). It is the Pomeron pole plus Pomeron-Pomeron cut piece of the total amplitude. Save for logarithmic factors which we ignore, this term has the same total s and subenergy dependences as the

unabsorbed $A_{0,P}$ term, Eq. (17), viz., $A_{0,P} \propto s_1 \sim s$. It is the dominant asymptotic contribution. The term in the second square brackets of Eq. (35) is the sum of the leading Regge ($\alpha_R \simeq 0.5$) pole part of the Deck amplitude, plus the two Pomeron-Regge cut terms. In applications of the Deck model to data in the conventional accelerator range of 5 to 30 GeV/c, the full πN elastic amplitude is used. Thus, in practice, these nonleading $s_1^{0.5+t_1}$ pole terms are retained and are relevant. The Pomeron-Regge cut terms have the s and s_{ij} dependences of

$$\frac{s_1}{s_{12}^{1/2}} \text{ and } s_1^{1/2},$$

respectively. Because $\langle s_{12} \rangle \simeq s$ and $\langle s_1 \rangle \propto s$, the Pomeron-Regge cut terms behave not unlike the Regge pole $s_1^{0.5}$ contribution in their effective s and subenergy dependences. Correspondingly, even after the Pomeron-Regge cut pieces are incorporated, we can again expect that absorption will yield at most minor modifications of, for example, the structure of the low-mass enhancement in the distribution, $d\sigma/dM_{a^*\pi}$.

The major effect of the Pomeron-Pomeron cut amplitude is to alter dramatically the momentum transfer distribution $d\sigma/dt_1$, as we described above, because it produces a zero in the full amplitude near $t_1 \simeq -0.3$ (GeV/c)^2. The addition of the Regge and Pomeron-Regge terms enhances this result, inasmuch as these terms should also have a zero near the same (perhaps even smaller) value of $|t_1|$. To arrive at this conclusion, we have only to examine the t dependences of the various Regge terms. The f_0 Regge amplitude is reputed[18] to have a t dependence similar to that of the Pomeron. If so, we may repeat the same calculation done for the Pomeron term, with the same resulting t_1 structure. The peripheral Regge exchanges (ω, ρ, A_2, and, perhaps, f_0) have a non-spin-flip amplitude[18] behaving in t_1 approximately as $A \sim (t_1 + 0.2\ \text{GeV}^2)$. Owing to this zero in the integrand, the convolution integral Eq. (3) will be small, thus leaving the zero in the total amplitude.

Because the behaviors of the asymptotic and nonasymptotic terms are similar in the essential t-dependent features of concern to us in this paper, we continue to work only with the leading asymptotic $[A_{0,P} + A_P \otimes A_{0,P}]$ term for the remainder of this article.

IV. MODELS FOR $NN \to NN\pi$ and $Kp \to K^*\pi p$

In Sec. III we used an exponential parametrization for the t dependence of the pion propagator in the Deck amplitude. As a result, we were able to express the absorptive corrections in a simple closed analytic form, whose qualitative and quantitative properties could be extracted almost by inspection. In this section we study amplitudes incorporating more realistic expressions for the pion propagator, Eqs. (13) and (14). We begin in Sec. IV A with a derivation appropriate to an arbitrary function $g(t_2)$ for the pion's t_2 dependence. In Sec. IV B we specialize to the reactions $pp \to p(n\pi^+)$ and $pn \to p(p\pi^-)$. In Sec. IV C we treat $Kp \to (K^*\pi)p$ and $\pi p \to (\rho\pi)p$.

A Arbitrary pion t dependence

We write the pion-exchange Deck amplitude corresponding to Fig. 1(a) as

$$A_0(s_1, t_2, t_1) = i\sigma^{\pi p} g(t_2) s_1 \exp(B_1 t_1). \tag{36}$$

Examples are given in Eqs. (13) and (14) of the function $g(t_2)$ which expresses the pion propagator dependence on t_2 as well as factors which arise from the coupling at the $(aa^*\pi)$ vertex. We ignore Reggeization of the pion, which would introduce dependence on s_2 into Eq. (36), as well as a t_2-dependence phase variation. These omissions are discussed below. They are inessential to the major conclusions of our present investigation. Retaining Eq. (9) for the elastic amplitude, we obtain from Eq. (3)

$$A_{\text{abs}}(s_1, t_2, t_1) = \frac{-i\sigma^{\pi p}\sigma^{a^* p} s_1}{8\pi^2} \times \int d^2\vec{q}_{3T}\, g(t_2')\exp(B_1 t_1' + B_3 t_3). \tag{37}$$

Expressions for t_1', t_2', and t_3 are given in Eqs. (4)–(7). We define a new variable for convenience:

$$\vec{V} = \vec{p}_{2T} + \frac{B_1}{(B_1 + B_3)}\vec{p}_{1T}. \tag{38}$$

As in Sec. III, $\vec{p}_{1T}$ and $\vec{p}_{2T}$ are the transverse components of the center-of-mass momenta of the final-state hadrons p and a^*, respectively. After minor algebraic manipulations and a change of integration variables in Eq. (37), we perform an angular integration analytically. The result is a one-dimensional integral expression for A_{abs}:

$$A_{\text{abs}}(s_1, t_2, t_1) = \frac{-\sigma^{a^* p}}{8\pi} \frac{A_0(s_1, t_2, t_1)}{g(t_2)} \times \exp\left[\frac{-B_1^2 t_1}{B_1 + B_3} - (B_1 + B_3)\vec{V}^2\right] \times \int dU^2 I_0[2(B_1 + B_3)U|\vec{V}|] \times g(t_2')\exp[-(B_1 + B_3)U^2], \tag{39}$$

$$t_2' = t_2 + \frac{1}{|\chi_2|}(\vec{p}_{2T}^{\,2} - U^2)$$

$$= -\frac{1}{|\chi_2|}U^2 + m_a^2(1-|\chi_2|) + m_{a*}^2(1-1/|\chi_2|). \quad (40)$$

In Eq. (39) the function I_0 is a modified Bessel function. It enjoys the properties

$$I_0(\chi) \to 1 \text{ as } \chi \to 0$$

and

$$I_0(\chi) \to \exp(\chi)/(2\pi\chi)^{1/2} \text{ as } \chi \to \infty.$$

The expression (39) for A_{abs} contains a one-dimensional integral which must be evaluated numerically. In Secs. IV B and IV C we select specific forms for $g(t_2')$, and discuss results. Beforehand, however, we comment briefly on modifications of Eq. (39) which result from Reggeization of the pion exchange.

Reggeization[8] of the pion introduces a factor of the type

$$[\tfrac{1}{2}(s_2 - u_2)]^{\alpha_\pi} e^{-i\pi\alpha_\pi} \quad (41)$$

in the unabsorbed Eq. (36). Here, α_π is the pion trajectory

$$\alpha_\pi = \alpha_\pi'(t_2 - m_\pi^2), \quad (42)$$

with slope α_π', and

$$u_2 = -s_2 - t_2 + t_1 + m_a^2 + m_{a*}^2 + m_\pi^2. \quad (43)$$

Note that this factor brings dependence on s_2 into Eq. (36) as well as a t_2-dependent phase variation. The Regge dependence on s_2 is instrumental in sharpening the theoretical distribution $d\sigma/dM_{a*\pi}$, bringing it more in accord with data, and it also generates the required asymmetry in the Treiman-Yang angular distribution in the final πp rest system.[8] Experimental tests of the $e^{-i\pi\alpha_\pi}$ phase variation are also discussed in Ref. 8.

Unfortunate technical disadvantages in the absorption convolution arise from including a factor of the type (41) into Eq. (36). As a result of the extra complexity, neither of the integrations in the two-dimensional convolution Eq. (3) can be done analytically. It is essentially for this reason that we have worked with the stripped-down version of the π-exchange Deck model, Eq. (36). Nevertheless, even if the Reggeized form were used in the convolution, important results would not change appreciably. For $Kp \to K^*\pi p$ at 40 GeV/c, we have computed distributions in mass, momentum transfer, and various decay angles generated from Eq. (36) and from the complete Reggeized amplitude. The momentum-transfer distributions, which are the most crucial in the convolution integral Eq. (3), are essentially indistinguishable quantitatively. The same remark applies to decay angular distributions in the $(K^*\pi)$ rest frame. The only spectra affected seriously are $d\sigma/dM_{K^*\pi}$ and the Treiman-Yang angle mentioned above. Therefore, we suggest that a convenient and reasonably reliable method for reintroducing Reggeization effects into the absorbed unReggeized calculation is simply to insert expression (41) as a multiplicative factor on the right-hand side of Eq. (39).

B. $NN \to NN\pi$

For $pp \to pn\pi^+$ [or $np \to (p\pi^-)p$], the factor $g(t_2)$ in Eqs. (36) and (39) is

$$g(t_2) = \sqrt{-t_2}\exp(t_2)/(m_\pi^2 - t_2). \quad (44)$$

The important terms in Eq. (44) are the pseudoscalar coupling factor $\sqrt{-t_2}$ and the pion propagator $(m_\pi^2 - t_2)^{-1}$. We ignore over-all coupling constants in this article. In Figs. 6–9 we compare various results obtained from our unabsorbed and absorbed models for $pp \to p(n\pi^+)$ at 100 GeV/c. The parameters $B_1 = 4.5$ (GeV/c)$^{-2}$, $B_3 = 5.5$ (GeV/c)$^{-2}$, and $\sigma^{np} \simeq 38$ mb $= 98$ GeV^{-2} are taken directly from elastic and total cross-section data. Therefore, the dip position in Figs. 6 and 7 and the slopes in Fig. 8 are absolute predictions. The agreement of the slopes in Fig. 8(a) with recent Fermilab neutron dissociation data[3] is excellent, and would seem to support the absorbed Deck picture strongly. We now turn to a more detailed examination of Figs. 6–9.

1. Helicity decomposition

In Fig. 6 we present the differential cross section $d\sigma/dtdM$ versus momentum transfer for the production of an $(n\pi^+)$ system of mass $M = 1.3$ GeV/c. Shown in Fig. 6(a) are the unabsorbed results, obtained from Eqs. (36) and (44), and in Fig. 6(b) the absorbed results obtained from

$$A = A_0 + A_{\text{abs}},$$

with A_{abs} given by Eqs. (39) and (44). For both the absorbed and unabsorbed differential cross section, we show the total $d\sigma/dtdM$, as well as a decomposition of this quantity into the portions for each of the spin and helicity states which contribute to the system of mass M (cf. Sec. III C 3). Indeed, the recoil system M in $pp \to pM$ is not in a state of unique spin, although the s-wave component is certaintly dominant. Our Deck amplitudes specify the relative strengths of the different spin states.

In Fig. 6 the partial-wave decomposition is presented in terms of s-channel helicities of system M (the quantization z axis is the direction of the final proton). In Fig. 7 the same decomposition is

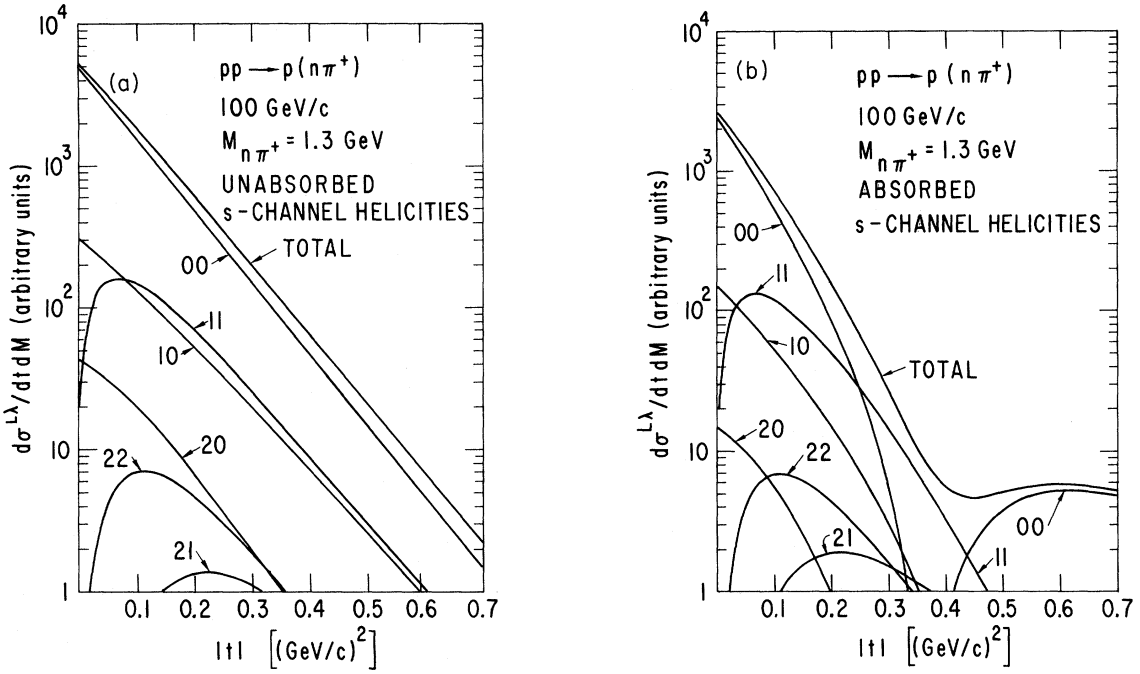

FIG. 6. Double differential cross section $d\sigma/dtdM$ for $pp \to p(n\pi^+)$ at 100 GeV/c and its decomposition into partial cross sections for individual spin-helicity states of the $(n\pi^+)$ system. Curves are obtained from the model of Sec. IV B. The states are labeled by the orbital angular momentum L and s-channel helicity λ_s of the $(n\pi^+)$ system, with the intrinsic spins of the nucleons ignored. For $\lambda_s \neq 0$, curves denote the sum of cross sections for (L, λ_s) and $(L, -\lambda_s)$. Results for the unabsorbed model are given in part (a); those for the absorbed model in (b). The over-all normalization is arbitrary, but the relative normalization of curves within part (a) and within part (b) is fixed by the model. The relative normalization between parts (a) and (b) is also determined by the model.

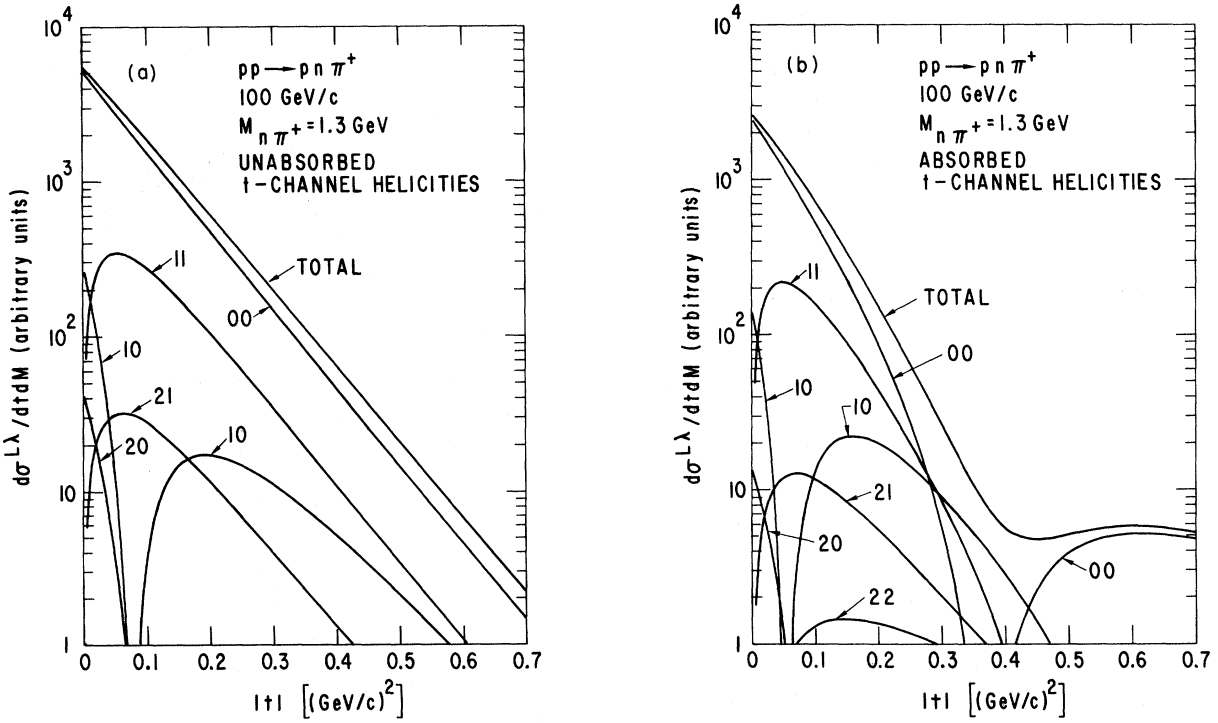

FIG. 7. As in Fig. 6, except that states of the $(n\pi^+)$ system are labeled by the t-channel helicity λ_t instead of λ_s.

made in terms of t-channel helicities [quantization axis along the initial proton which dissociates into $(n\pi^+)$]. We have ignored intrinsic spins of particles. Therefore, the spin, helicity labels refer to orbital angular momentum only in the rest system of M. The quantity labeled σ^{11} is the sum of σ^{11} and $\sigma^{1,-1}$.

A comparison of Figs. 6(a) and 6(b) shows that the amplitudes with s-channel helicity $|\lambda_s| \geq 1$ are not much absorbed. The states with $\lambda_s = 0$ suffer the greatest absorption. At $M_{\pi^* n} = 1.3$ GeV, in the state $(L=0, \lambda_s=0)$, a zero of the full amplitude is generated at $|t| = 0.37$ (GeV/c)^2. The zero locations of some other amplitudes are listed in Table I, for three values of mass. These explicit zero locations correspond crudely but not exactly to positions conjectured in *ad hoc* geometric models.[6,13] Most notable is the fact that all zero locations move to larger $|t|$ as M increases. In impact-parameter language, this means that for fixed (L, λ) states of higher mass are produced less peripherally in our model. As a result of this motion of the zero location with M, structure in $d\sigma/dtdM$ is washed out if a relatively large interval (e.g. $\Delta M \gtrsim 0.5$ GeV) in M is averaged or integrated over. Thus, even $d\sigma^{L,\lambda_s}/dtdM$ for a specific (L, λ_s) state may show little or no structure in t if too large an interval in M is selected in the data.

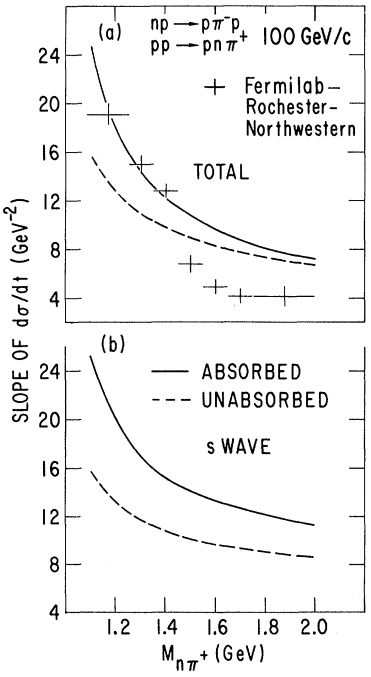

FIG. 8. Logarithmic slope of the momentum transfer t_{pp} dependence for nucleon dissociation $Np \to (N\pi)p$ at 100 GeV/c as a function of the mass of the $(N\pi)$ system. Results are shown for (a) the total cross section $d\sigma/dtdM$ and (b) the $(N\pi)$ s-wave component. Data from Ref. 3 on neutron dissociation are listed in (a).

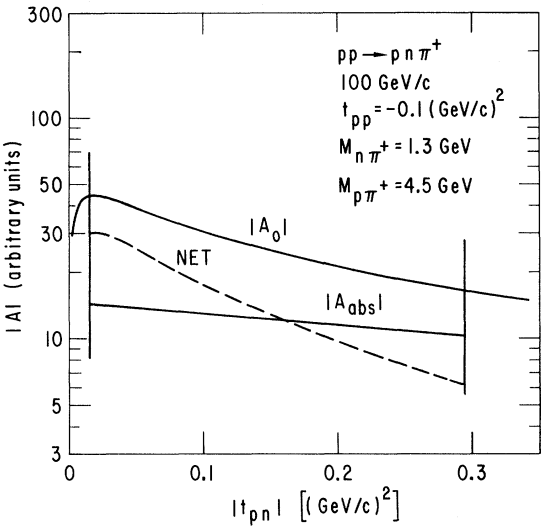

FIG. 9. Absolute values of the unabsorbed Deck amplitude A_0, the absorption term A_{abs}, and the net amplitude $A_0 + A_{abs}$ as a function of the momentum transfer t_{pn}. The fixed values of the other variables are listed. The vertical bars denote the boundaries of the kinematically allowed region. Note the turnover in A_0 at small t_{pn} which arises from the $(-t_{pn})^{1/2}$ factor.

In Fig. 6(b) we note that the $(L=1, \lambda_s=1)$ amplitude fills in the pronounced dip in $d\sigma/dt$ near $t = 0.4$ (GeV/c)^2 which would occur if only the $(L=0)$ state were present. The dip is partially removed by a state of different s-channel helicity. In the unabsorbed results, Fig. 6(a), the ratio σ^{00}/σ^{11} is roughly 6 at $|t| = 0.4$ (GeV/c)^2. However, roles are entirely reversed in the absorbed model, with the $(L=1, \lambda_s=1)$ state being overwhelming near this value of $|t|$. At small $|t|$, say $t = -0.1$ (GeV/c)^2,

TABLE I. Locations in $|t_1|$ of the zeros in the amplitudes for producing various states of s-channel spin and helicity (L, λ_s) are given as a function of mass M of the $(n\pi^+)$ system, from our absorbed Deck model of $pp \to p(n\pi^+)$ at 100 GeV/c. The first column lists values of (L, λ_s). Dip positions [in (GeV/c)^2] for three different mass values are listed in columns 2–4.

$L\lambda_s$ \ $M_{n\pi^+}$	1.1 GeV	1.3 GeV	1.5 GeV
00	0.29	0.37	0.43
10	0.33	0.47	0.63
11	0.48	0.67	0.80
20	0.17	0.33	0.45
21	0.63	>1	>1
22	0.66	0.93	>1

we note that in our unabsorbed model, the ratio of helicity 1 cross sections is roughly 14 (factor $\simeq 3.7$ in amplitude) whereas in the absorbed model the ratio is 6.6 (factor of 2.6 in amplitude).

We note that the two dominant amplitudes in Fig. 6(b) have $(L, \lambda_s) = [0, 0]$ and $[1, 1]$. Because the $[0, 0]$ amplitude vanishes near $t = -0.4$ $(\mathrm{GeV}/c)^2$, the interference term in the cross section between the $[0, 0]$ and $[1, 1]$ waves changes sign at this value of t_1. Therefore, a prediction of our model is that the moment $\langle Y_{11} \rangle$ of the cross section changes from positive to negative (with our convention for defining angles) close to this value of t_1. Statements about other moments are ambiguous because many small partial waves contribute.

In the t-channel helicity decomposition of Fig. 7(a), apparently bizarre effects show up in the unabsorbed model. Indeed, the $(L = 1, \lambda_t = 0)$ and $(L = 2, \lambda_t = 0)$ unabsorbed amplitudes both vanish at $|t| \simeq 0.1$ $(\mathrm{GeV}/c)^2$. These appear to be largely kinematic accidents to which we attach no significance. We do not comment in detail on Fig. 7, but we include it here for completeness. A series of remarks analogous to those made above for Fig. 6 could be repeated.

2. Mass-slope correlation

In Fig. 8 we present the variation with $M_{n\pi^+}$ of the small t slopes of $d\sigma/dtdM_{n\pi^+}$. The slope b is defined through the parametrization

$$\frac{d\sigma}{dtdM} \propto \exp(bt).$$

Fits were made over the range $0.05 \leq |t| \leq 0.2$ $(\mathrm{GeV}/c)^2$. The comparison of absorbed and unabsorbed results in Fig. 8(a) indicates that absorption increases the threshold value of the slope by roughly 9 units, but causes only a modest increase at $M_{n\pi^+} \simeq 2$ GeV. Absorption accentuates the pronounced mass-slope correlation already present in the unabsorbed model (cf. Sec. III C for a qualitative discussion). On Fig. 8(a) we have placed slope values obtained in a recent Fermilab experiment[3] on $np \to (p\pi^-)p$. The excellent agreement with our absolute predictions in the mass range up to 1.4 GeV seems to support strongly the Deck interpretation of kinematic nature of low-mass threshold enhancement, as well as the need for absorptive corrections in the model. At larger $M_{p\pi^-}$, from 1.5 to 2.0 GeV, the model disagrees with data. However, we call attention to the fact that in this region, obvious resonance effects are observed in the data. They are not included in the model. The resonances appear to be produced with a t slope which is substantially smaller than that of the diffractive Deck background.

In Fig. 8(b) we present the slope of $d\sigma^{00}/dtdM$. This is the differential cross section for producing the s-wave part only of the Deck enhancement. We observe that there is a pronounced mass-slope correlation in both the unabsorbed and absorbed results. Although perhaps of somewhat esoteric interest now, we include these results in the expectation that data will soon be available. The results of Fig. 8(b) demonstrate that in our model the mass-slope correlation is present already in the dominant $L = 0$ partial wave, all by itself.

An alternative interpretation[6,13] of the mass-slope correlation has been suggested repeatedly. In these approaches the mass-slope correlation owes its existence to the presumed growth with M of higher L and λ_s states, produced with systematically smaller slopes b. For a given (L, λ_s), the slope b is assumed not to vary with M. While perhaps intuitively appealing, the approach suffers from a surplus of undetermined parameters and has not been tested quantitatively. It seems to us unlikely that the data (particularly the distribution in ϕ_s) would tolerate an increase of λ_s with M sufficiently rapid to achieve the result desired. In any case, the issue can be resolved experimentally. Some data on the mass-slope correlation in the $L = 0$ partial wave in $\pi p \to (\rho\pi)p$ at 40 GeV/c have been published.[19] A decrease of slope from 12 ± 1 to 7 ± 1 $(\mathrm{GeV}/c)^{-2}$ is observed (cf. Table 1, p. 157 of Ref. 19) from $M_{\rho\pi} = 1.1$ to 1.3 GeV. Therefore, available results, while sketchy, surely are consistent with our viewpoint that the mass-slope correlation is an intrinsic property of each partial wave.

3. Distribution in t_2

The unabsorbed amplitude Eq. (44) vanishes as $\sqrt{-t_2}$ as t_2 approaches zero. As a result of absorption, this effect is partially removed. In Fig. 9 we present curves which show the magnitude of the unabsorbed and absorbed amplitudes as a function of $|t_{pn}|$ for the process $pp \to p(n\pi^+)$ at 100 GeV/c. The fixed values selected for the other three invariants are indicated. The physically allowed interval of t_{pn} is denoted by the vertical bars. At $M_{n\pi^+} = 1.3$ GeV and the (rather typical) $|t_{pp}| = 0.1$ $(\mathrm{GeV}/c)^2$, $|A_{\mathrm{abs}}| \lesssim 0.3|A_0|$, as may be seen by comparing Figs. 6(a) and 6(b). Figure 9 shows that $|A_{\mathrm{abs}}|$ is fairly constant in t_{pn}, dropping only gradually as $|t_{pn}|$ increases. Owing to the different t_{pn} dependence of the unabsorbed amplitude, the net effect of absorption is to generate a fairly steep t_{pn} dependence in the full amplitude $|A| = |A_0 + A_{\mathrm{abs}}|$. Indeed, it is amusing to note that the net amplitude in Fig. 9 falls with t_{pn} roughly as $m_\pi/(m_\pi^2 - t_{pn})$ in the physical region, just as if the full effect of absorption were to have been the simple

replacement[20] of $\sqrt{-t_2}\exp(t_2)$ by m_π in the unabsorbed amplitude. We regard this numerical coincidence as purely fortuitous. It makes little if any sense physically. Moreover, at larger $|t_{pp}|$, where the absorptive effects are much greater, the algorithm may not even work numerically.

C. $\pi p \to \rho\pi p$ and $Kp \to K^*\pi p$

The structure in momentum transfer t_2 of the pion-exchange Deck amplitude [Fig. 2(a)] for $Kp \to K^*\pi p$ or for $\pi p \to \rho\pi p$ is relatively simple. In addition to the pion propagator $(m_\pi^2 - t_2)^{-1}$, there may be a mild (e.g., exponential) form factor, but there is no significant coupling factor as in $NN \to NN\pi$ which alters the behavior near $t_2 = 0$. Therefore, for $g(t_2)$ in Eq. (36) and in Eq. (39), we take

$$g(t_2) = \frac{1}{(m_\pi^2 - t_2)} .$$

Results of our numerical investigation for $Kp \to K^*\pi p$ at 40 GeV/c are presented in Figs. 10–12. The parameters appropriate in this case are $B_1 = 4$ (GeV/c)$^{-2}$, $B_3 = 4$ (GeV/c)$^{-2}$, and $\sigma_{K^*p} \simeq \sigma_{Kp} = 18$ mb = 46 GeV. In selecting B_3 and σ_{K^*p}, we used experimental values for the Kp elastic and total cross sections at 40 GeV/c. The value $B_1 = 4$ is the experimental slope of the πp elastic differential cross section at $s_1 \simeq s/4 = 20$ GeV^2.

As noted in Eq. (39), the strength of the absorption term is proportional to σ^{a^*p}. Because $\sigma^{Kp} \lesssim \frac{1}{2}\sigma^{np}$, absorptive effects are weaker for $Kp \to K^*\pi p$ than for $pp \to p n\pi^+$. One practical result of this difference is that the absorption dip in $d\sigma/dt_{pp}$ is displaced from $|t_{pp}| \simeq 0.4$ to 0.6 (GeV/c)^2 in the model, as is seen from a comparison of Figs. 6(b) and 10(b).

In Figs. 10(a) and 10(b) we compare $d\sigma/dtdM$ for our absorbed and unabsorbed models of $Kp \to K^*\pi p$ at 40 GeV/c. The chosen value $M_{K^*\pi} = 1.3$ GeV is roughly the central point of the low-mass $(K^*\pi)$ enhancement (Q bump) generated in the model. The decomposition of $d\sigma/dtdM$ into portions associated with different (L, λ) values of the $(K^*\pi)$ system is also presented. For this reaction we limit our presentation to a figure with the t-channel helicity decomposition. Remarks analogous to those made above for the helicity decomposition of $pp \to pn\pi$ may be repeated here.

In Fig. 11 we show the $(K^*\pi)$ mass dependence of the slope of $d\sigma/dt$ for both our absorbed and unabsorbed models. Again, there is a pronounced mass-slope correlation for the total amplitude, as well as for the dominant s-wave part. Absorption accentuates the correlation. Data points in Fig. 11(a) from a Serpukhov experiment[21] are in closer agreement with the unabsorbed expectations. In this connection, we remark that an examination of

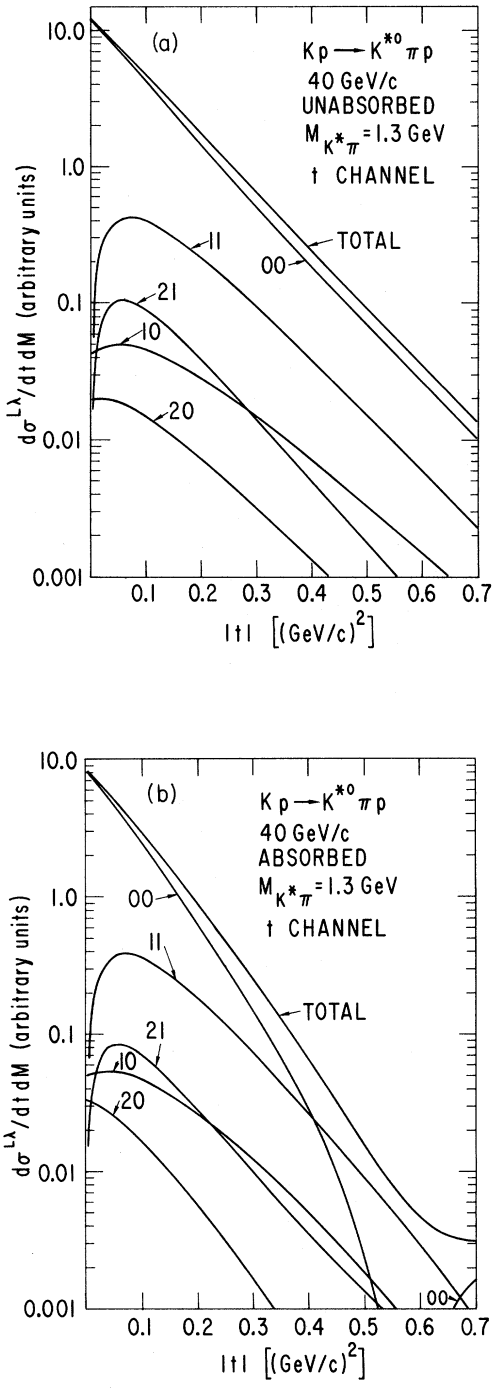

FIG. 10. Double differential cross section $d\sigma/dtdM$ for $Kp \to K^*\pi p$ at 40 GeV/c and its decomposition into partial cross sections for individual t-channel spin-helicity states of the $(K^*\pi)$ system. The spin of the K^* is neglected. States are labeled by orbital angular momentum and t-channel helicity λ_t. Results correspond to the model described in Sec. IV C; part (a) for the unabsorbed model, and part (b) for the absorbed version.

the s-channel azimuthal angular distribution of the K^* from 8–14 GeV/c $K^-p \to (K^*\pi^-)p$ data suggests equal contributions from the K^* and π-exchange Deck graphs.[8] The K^* graph has a much weaker mass-slope correlation. When both K^* and π contributions are properly included, the unabsorbed and absorbed curves in Fig. 11(a) should both drop. Similar depression is not expected to be significant in the $NN \to NN\pi$ case because the baryon exchange "u-channel" contribution appears to be less than half as great as the pion contribution.

In Fig. 12 results are presented as a function of the $(K^*\pi)$ invariant mass. Cross sections have been integrated over t_1. Displayed in Fig. 12(a), for the unabsorbed model, is the decomposition of the cross section into contributions from various s-channel partial waves. The $L=0$ wave is dominant over the full range shown, $M_{K^*\pi} \leq 2$ GeV, with the $(L=1, \lambda_s=1)$ wave in second place. The effects of absorption on these two leading amplitudes are presented in Fig. 12(b). The cross section in the $L=0$ state is reduced by nearly a factor of 2, whereas the $(L=1, \lambda_s=1)$ cross section decreases only to ~85% of its unabsorbed value.

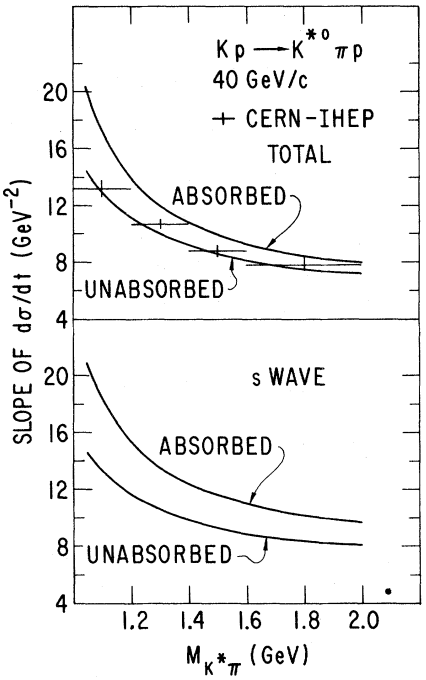

FIG. 11. Logarithmic slope of the momentum transfer t_{pp} dependence for $Kp \to (K^*\pi)p$ at 40 GeV/c as a function of the mass of the $(K^*\pi)$ system. Results are shown for (a) the slope of the total $d\sigma/dtdM$ and (b) the $(K^*\pi)$ s-wave portion. Data from Ref. 21 are indicated in (a). Slopes are determined over the t_{pp} interval $0.05 \leq |t_{pp}| \leq 0.30$ (GeV/c)^2.

V. CONCLUSIONS AND DISCUSSION

In this article we investigated in detail absorptive corrections to the Deck model for diffraction dissociation. After establishing which absorptive terms are appropriate physically, we demonstrated that absorption of the expected strength reproduces quantitatively the mass-dependent structure in momentum transfer observed in the Fermilab data[3] on diffractive neutron dissociation $np \to (p\pi^-)p$ and ISR data[2] on proton dissociation $pp \to p(n\pi^+)$. This agreement supports the Deck in-

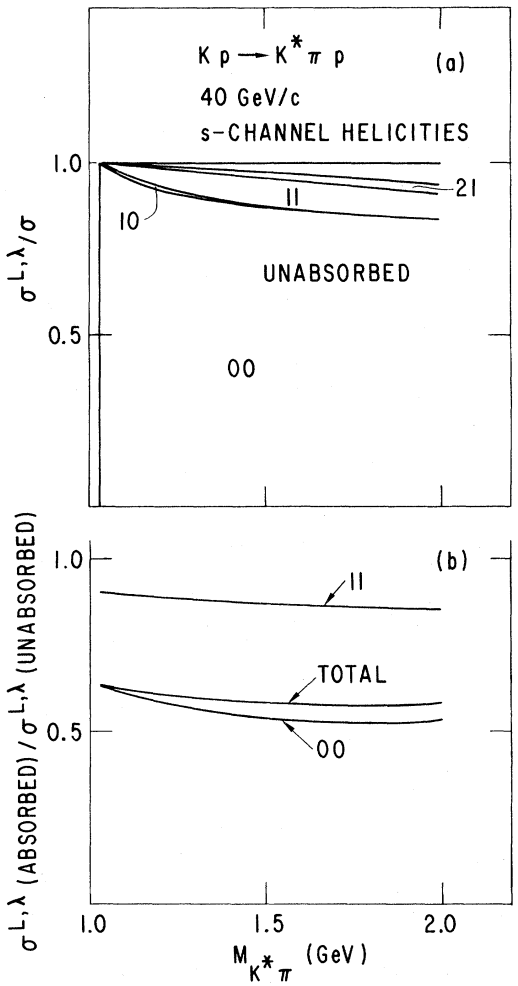

FIG. 12. (a) Relative cross sections for the production of different (L, λ_s) states of the $(K^*\pi)$ system in $Kp \to K^*\pi p$ at 40 GeV/c are plotted as a function of $(K^*\pi)$ mass. These values are obtained from the unabsorbed π-exchange Deck model of Sec. IV C. The label (11) denotes the sum $\sigma^{11}+\sigma^{1,-1}$, and (21) refers to $\sigma^{21}+\sigma^{2,-1}$. (b) The reduction of the cross section as a result of absorption is shown as a function of $(K^*\pi)$ mass for the total cross section and for the two dominant partial cross sections.

terpretation of the kinematic nature of diffractive threshold enhancements and the necessity for absorptive corrections to the model. There are no undetermined parameters in our approach. The structure in $d\sigma/dtdM$ at small t indicates that diffraction dissociation is a peripheral process in impact parameter, whereas elastic diffraction is central.

We decomposed our full amplitude for the process $ap \to Mp$ into partial amplitudes for each of the angular momentum and helicity states which contribute to the system M. We showed how absorption affects each of these partial amplitudes individually. For the dominant $L=0$ amplitude, absorption generates a zero at small $|t|$, which moves to larger $|t|$ as M increases. At fixed M, a pronounced minimum at a well-defined $|t|$ value is predicted for the dominant partial cross section $d\sigma^{L=0}/dtdM$. At fixed M, this dip is partially filled in by contributions from higher-L states, when the full distribution $d\sigma/dtdM$ is examined. Whether one selects a partial cross section or the full $d\sigma/dtdM$, the structure predicted in t is washed out if too large an interval in M is averaged over in the data. This happens as a result of the displacement of structure to larger $|t|$ as M increases. High-statistics data with good mass resolution are crucial.

In examining $d\sigma/dt\,dM$ at small t, we find that there is a pronounced decrease of the slope in t with increasing M. This mass-slope correlation is present in the unabsorbed Deck model, but it is considerably accentuated in the absorbed model (Figs. 8 and 11). We note also that the mass-slope correlation is a property of the dominant $L=0$ partial wave in both the absorbed and unabsorbed models. In other words, in our model a strong decrease of production slope with mass occurs even if only the dominant $L=0$ wave were present in the data. This contrasts with other approaches[6,13] in which the mass-slope correlation owes its existence to the presumed increase with M of contributions from states of higher L and helicity. The two viewpoints can be tested by partial-wave analyses of inelastic diffractive data. Present sketchy results[19] support our viewpoint.

As just summarized, the most dramatic effects of absorption are seen in the production t distribution $d\sigma/dMdt$. The integrated mass distribution $d\sigma/dM$ shows little modification in shape in the small M region of interest here. The over-all integrated cross section is reduced to roughly one-half its unabsorbed value. At small t, the decay angular distributions in the rest frame of M are essentially unchanged by absorption. At larger $|t|$, [$\gtrsim 0.3$ (GeV/c)^2], where the absorption term and the unabsorbed amplitude are of comparable magnitude, the predicted partial-wave structure is modified appreciably. Figures 6, 7, and 10 may be consulted for numerical estimates. Insofar as statistics allow, it is advisable to perform experimental partial-wave analyses of the system M in several different regions of $|t|$. If all $|t|$ values are included, little difference is seen between the absorbed and unabsorbed models.

In our calculations, we worked with somewhat simplified versions of the pion-exchange Deck amplitude, and we considered only elastic absorption. If inelastic intermediate states are introduced into the absorption convolution, the over-all effect of absorption becomes stronger. On the other hand, if Regge phases and all spin effects are included in the Deck amplitude, the resulting incoherence reduces the final absorptive effects.

Certain predictions based on the unabsorbed Deck model must be reevaluated in the light of our present conclusion that absorptive corrections are necessary. Several of these issues have already been treated above. We include brief remarks here on two other questions. Nucleon polarization effects were discussed by Berger and Fox.[22,8] As a result of absorption, the effective Pomeron in inelastic diffraction has structure in t which is considerably different from that in elastic scattering. The inelastic Pomeron amplitude passes through zero near $|t|=0.3$ (GeV/c)^2, whereas the elastic Pomeron amplitude is apparently featureless out to $|t|\simeq 1$ (GeV/c)^2. This structure is reflected in the t dependence of the inelastic polarization. Thus, rather than the positive polarization, with a double zero near $|t|\simeq 0.6$ (GeV/c)^2, expected previous[22,8] for $pp \to p(n\pi^+)$, we now expect a change of sign of polarization from positive to negative near $|t|=0.3$ (GeV/c)^2. The location of this zero moves to larger $|t|$ as $M_{n\pi^+}$ is increased. When integrated over $|t|$, the polarization as a function of $M_{n\pi^+}$ will also be smaller, owing to this sign change. This may explain the small polarization[23] observed in inclusive reactions $pp \to pX$ at small M_X. We can only urge again that detailed polarization data as a function of t and M in selected exclusive inelastic diffraction dissociation processes should be of great assistance in further defining the dynamics of quasielastic reactions. Experiments with the Argonne polarized proton beam are of obvious interest.

The second remark pertains to crossovers in t of the differential cross sections observed when data are compared for pairs of reactions related by charge conjugation in the t channel. A detailed study of this subject was published[17] in the context of the unabsorbed Deck model. An interesting example is the pair $K^0p \to Q^0p$ and $\overline{K}^0p \to \overline{Q}^0p$, for which the unabsorbed pion-exchange Deck graphs

are given in Fig. 13. These pion-exchange Deck graphs predict that at $t=0$, $d\sigma/dt\,(K^0) > d\sigma/dt(\bar{K}^0)$, because $\sigma(\pi^- p) > \sigma(\pi^+ p)$. They also predict that the slope of $d\sigma/dt(K^0)$ > slope of $d\sigma/dt(\bar{K}^0)$, because this is true of the slopes of the $\pi^+ p$ elastic scattering amplitudes which are imbedded in the Deck graphs. These two expectations disagree with data,[24] for which just the opposite results are true.

Absorption involves rescattering of the final $K^* p$ and $\bar{K}^* p$ systems. Because the nonexotic $K^{*-} p$ total cross section is presumably greater than the exotic $K^{*+} p$ total cross section, just as $\sigma^{K^- p} > \sigma^{K^+ p}$, we expect the absorptive effects to be stronger in the $\bar{K}^0 p$ reaction than in $K^0 p$. These reduce the $t=0$ value of the $\bar{K}^0 p$ cross section relative to that for $K^0 p$. Unfortunately, this goes in just the wrong direction to remedy one of the discrepancies with the data. Absorption increases the *slope* of $d\sigma/dt(\bar{K}^0)$ relative to that of $d\sigma/dt(K^0)$, counteracting the tendency of the unabsorbed amplitude, but its effect on the magnitude of the cross section destroys the cross-over. In our view,[8,17] a proper description of the cross-over requires including both the K^*- and π-exchange Deck amplitudes. This conclusion is, if anything, strengthened by our present demonstration that absorption alone is not the answer to the cross-over problem.

ACKNOWLEDGMENTS

We have benefited from conversations with J. Dash, J. Pumplin, and T. Ferbel.

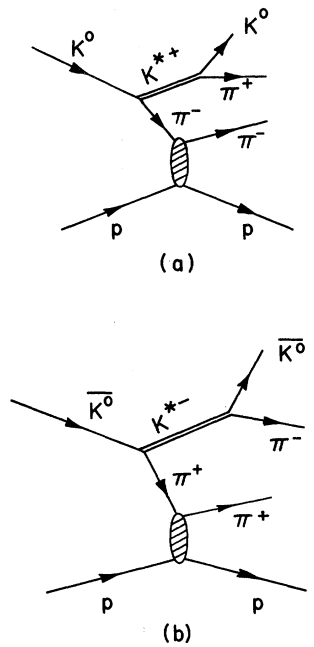

FIG. 13. Pion-exchange Deck graphs for the processes (a) $K^0 p \to K^{*+} \pi^- p$ and (b) $\bar{K}^0 p \to K^{*-} \pi^+ p$.

APPENDIX A: OPTICAL PICTURE OF DIFFRACTION DISSOCIATION

In this appendix we derive a model for the diffractive production of particles at high energy based on the Good and Walker[11] picture of diffraction dissociation. Our approach here is similar in some respects to that of Białas, Czyż, and Kotański.[11] We consider the scattering of any hadron a on any target, t, so that the initial state consists of a and t. For convenience, we make certain simplifying but inessential assumptions. We imagine that target t has no diffractive excitations. Second, we assume that hadron a can couple diffractively to itself, ψ_a, and to only one other state ψ_b. [As an explicit example, $a=p$ and $b=(n\pi^+)$]. Finally, we work in only one dimension.

Diffraction is defined to be pure shadow scattering of orthogonal states ϕ_1 and ϕ_2, which means that under diffraction $\phi_1 \to \eta_i \phi_i$ where the η_i are real numbers, $0 \leq \eta_i \leq 1$. The states ψ_a and ψ_b are linear combinations of ϕ_1 and ϕ_2:

$$\psi_a = \alpha_1 \phi_1 + \alpha_2 \phi_2 ,$$
$$\psi_b = -\alpha_2 \phi_1 + \alpha_1 \phi_2 . \tag{A1}$$

We have chosen the phases such that α_1 and α_2 are real. All states are normalized, $\alpha_1^2 + \alpha_2^2 = 1$.

If the initial state $\psi_{\text{in}} = \psi_a$, it is transformed under scattering into

$$\psi_{\text{out}} = \alpha_1 \eta_1 \phi_1 + \alpha_2 \eta_2 \phi_2 + \psi_{\text{ND}}. \tag{A2}$$

The nondiffractive wave ψ_{ND} is orthogonal to ϕ_1 and ϕ_2. The elastic scattering amplitude is obtained in the usual fashion as

$$iA^{\text{el}} = \psi_a^\dagger (\psi_{\text{out}} - \psi_a)$$
$$\equiv \eta_a - 1. \tag{A3}$$

Here,

$$\eta_a = \alpha_1^2 \eta_1 + \alpha_2^2 \eta_2 . \tag{A4}$$

Similarly, the inelastic diffractive amplitude is

$$iA^D = \psi_b^\dagger \psi_{\text{out}}$$
$$= \alpha_1 \alpha_2 (\eta_2 - \eta_1). \tag{A5}$$

Note that the inelastic diffractive amplitude is zero unless $\eta_2 \neq \eta_1$.

We assume next that $\alpha_1 \gg \alpha_2$, which is to say that states ϕ_1 and ϕ_2 are approximately equal to ψ_a and ψ_b, respectively. By virtue of the normalization condition, this means $\alpha_1 \cong 1$, $\eta_a \cong \eta_1$, and $\eta_2 \cong \eta_b = \alpha_1^2 \eta_2 + \alpha_2^2 \eta_1$. Note that η_1 and η_2 and, hence, A^D are determined quantities once the elastic scattering amplitudes are measured for ψ_a and ψ_b. The assumption $\alpha_1 \gg \alpha_2$ is motivated by the fact that the inelastic diffractive cross section to state b is smaller than the elastic cross section.

In order to connect the above discussion to the processes $ap \to (a^*\pi)p$ of interest in this article, we identify ψ_a as the incoming hadron state a and ψ_b as the $(a^*\pi)$ system. To achieve the one-dimensional picture, we take the a^* and π to be in a state of fixed longitudinal momenta and fixed relative transverse position. At high energies, this relative position does not change appreciably during interaction with the target. Finally, we must fix the impact parameter $\vec{b}$ of the collision. If the fractional longitudinal momenta of a^* and π are $\chi_2 = p_{a^*}/p_{\text{c.m.}}$ and $\chi_3 = p_\pi/p_{\text{c.m.}}$, the equation

$$\vec{b} = \chi_2 \vec{b}_2 + \chi_3 \vec{b}_3 \tag{A6}$$

relates the impact parameter of incident hadron a to those of hadrons a^* and π.

The amplitude for $(a^*\pi)$ elastic scattering is not known, of course. To get around this problem, we assume that the transmission strength of the $(a^*\pi)$ system is the product of the strengths of the particles individually:

$$\eta_2 = \eta_{a^*}(b_2)\eta_\pi(b_3). \tag{A7}$$

Equation (A5) can then be rewritten as

$$iA^D(\chi_1, \chi_2, \vec{b}_1, \vec{b}_2) \cong \alpha_2(\chi_1, \chi_2, \vec{b}_1, \vec{b}_2) \times [\eta_{a^*}(\vec{b}_2)\eta_\pi(\vec{b}_3) - \eta_a(\vec{b})]. \tag{A8}$$

This expresses the diffractive amplitude for producing the $(a^*\pi)$ state. Possible dependence of the η_i on χ_i and χ_2 has been suppressed. Replacing the η_i by the elastic scattering amplitudes [cf. Eq. (A3)], we rewrite the term in square brackets in Eq. (A8) as

$$\eta_{a^*}\eta_\pi - \eta_a = i(A_\pi^{\text{cl}} + A_{a^*}^{\text{cl}} - A_a^{\text{cl}}) - A_\pi^{\text{cl}} A_{a^*}^{\text{cl}}. \tag{A9}$$

The factor α_2 in Eq. (A8) contains both the $aa^*\pi$ coupling constant and the two-dimensional Fourier transform of the propagator of the $(a^*\pi)$ state. For elementary particles this propagator is

$$\Delta = (M_{a^*\pi}{}^2 - m_a{}^2)^{-1}. \tag{A10a}$$

Straightforward calculations allow Δ to be reexpressed at high energies as

$$\Delta = \frac{\chi_3}{m_\pi{}^2 - t_2}, \tag{A10b}$$

or as

$$\Delta = \frac{\chi_2}{m_{a^*}{}^2 - u_2}, \tag{A10c}$$

where the momentum transfers $t_2 = (p_{a^*} - p_a)^2$, and $u_2 = (p_\pi - p_a)^2$. Equations (A10b) and A(10c) are just the propagators of the off-shell π and a^*, respectively, in Figs. 2(a) and 2(b). Consequently, the first three terms in Eq. (A9) can be identified with the single-scattering graphs (a)–(c) in Fig. 2. The last term in Eq. (9) is the sum of the absorption graphs Figs. 3(c) and 3(d). (Both time orderings are clearly included.)

In this picture we observe that absorption graphs Figs. 3(a) and 3(b) correspond to a situation in which the transition $a \to (a^*\pi)$ occurs inside the target, a case which is clearly not important at high energy.

APPENDIX B: CALCULATION OF SOME ABSORPTION TERMS

In this appendix we discuss the calculation of absorption terms represented by Figs. 14(a)–14(d). The calculation is done to leading order in s. We include only the elastic intermediate state, meaning that intermediate-state particles a', $a^{*\prime}$, and p' are represented by an elementary particle propagator,

$$\Delta_i(y-x) = \theta(y_0 - x_0) \int \frac{d^4p}{(2\pi)^4} e^{-ip\cdot(y-x)} \frac{1}{p^2 - m_i{}^2 + i\epsilon} = \theta(y_0 - x_0) \times \int \frac{d^4p}{(2\pi)^4} e^{-ip\cdot(y-x)} 2\pi i\, \delta(p^2 - m_i{}^2)\theta(p_0), \tag{B1}$$

where m_i is m_a, m_{a^*}, or m_p.

The $\theta(y_0 - x_0)$ function is included because we want to retain the contribution only of the particle pole, at $p_0 = +(m_i{}^2 + \vec{p}^2)^{1/2}$. The first expression in Eq. (B1) leads to the same final result (to leading order in s) with or without this θ function, but this is not true for the second expression. Therefore, inclusion of the θ function is essential.

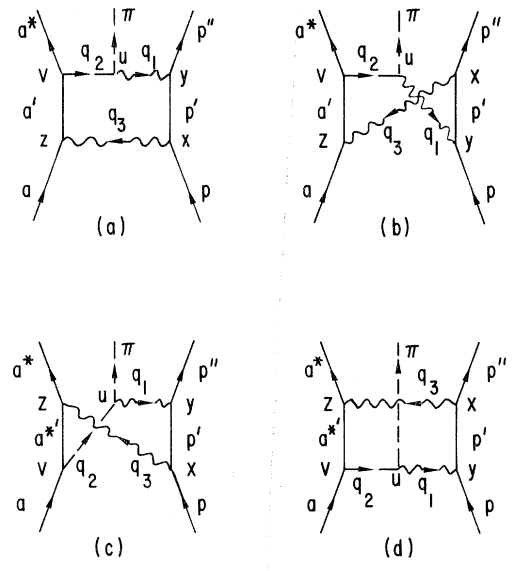

FIG. 14. Kinematic variables for the four absorption graphs discussed in Appendix B.

At high energies it is useful to use light-cone variables:

$$p_\pm = \frac{1}{\sqrt{2}}(p_0 \pm p_3),$$

$$x_\pm = \frac{1}{\sqrt{2}}(x_0 \pm x_3). \tag{B2}$$

For fast forward moving particles,

$$p_+ \approx p_0\sqrt{2},$$
$$p_- \approx (m^2 + p_T^2)/2p_+, \tag{B3}$$

$$x_+ \approx \text{const} + x_0\sqrt{2},$$
$$x_- \approx \text{const}. \tag{B4}$$

For backward moving particles, the roles of p_+ and p_- (x_+ and x_-) are interchanged. We work in the center-of-mass frame with particles p and p'' moving backward and a, a^*, and π forward. In terms of light-cone variables,

$$p^2 = 2p_+p_- - p_T^2, \tag{B5}$$

$$p \cdot x = p_+x_- + p_-x_+ - \vec{p}_T \cdot \vec{x}_T. \tag{B6}$$

The θ function $\theta(y_0 - x_0)$ can be replaced by $\theta(y_+ - x_+)$ ($\theta(y_- - x_-)$) for the forward (backward) moving particles.

Excluding corrections of order $1/s$ due to the small differences in the momenta of p and p'', we see that graphs (a) and (b) differ only by the sign of the argument in the θ functions $\theta(y_0 - x_0)$ and $\theta(x_0 - y_0)$. Therefore, their sum contains no θ function in $(y_0 - x_0)$. It can be represented by graph (a) with a simple on-shell propagator for particle p'. A similar result is true for the sum of graphs (c) and (d). Because the p_+ component of the momenta p_p, p'_p, and p''_p are of order $1/\sqrt{s}$, we find also that the momentum transfers $q_{1+} \sim 1/\sqrt{s}$, and $q_{3+} \sim 1/\sqrt{s}$. Therefore, the cutoff in q_{3-}, provided by the q_1 and q_3 propagators, does not occur until $q_{3-} \sim \sqrt{s}$. (We select q_3 as the independent integration variable, $q_1 = p_1 - p_a + q_3$.) Transforming back to space-time, we see that

$$z_+ - u_+ \sim \frac{1}{\sqrt{s}}. \tag{B7}$$

This result can be understood heuristically as a consequence of the Lorentz contraction of particle a. The momentum component $p_{\pi+}$ of the final-state pion is of the order $\sqrt{s}$ (although reduced by a factor of order m_π/m_{a^*}). Because q_{1+} is small, we see that $q_{2+} \approx p_{\pi+}$ is large; q_{2-} has to be small to keep q_2^2 small. It follows that the exchanged pion is moving forward, and only the time ordering $u_+ \gtrsim v_+$ gives an important contribution. (In other words, only the particle pole at $q_{2-} \approx 0 - i\epsilon$ is important, while the contribution of the antiparticle pole at $q_{2+} \approx 0 + i\epsilon$, q_{2-} large and negative, is strongly suppressed.) By Eq. (B7) $u_+ \gtrsim v_+$ leads to $z_+ \gtrsim v_+$. Therefore, graphs (a) and (b), which contain the factor $\theta(v_+ - z_+)$, do not contribute to leading order in s. On the other hand, the factor $\theta(z_+ - v_+)$ in the sum of graphs (c) and (d) can be dropped because the argument of θ is always positive. On the basis of the above arguments, we describe the total contribution of graphs (a)–(d) by Eq. (3) of Sec. II.

---

*Work performed under the auspices of the United States Energy Research and Development Administration.

[1]For reviews consult the articles by M. Derrick and A. N. Diddens, in *Proceedings of the XVII International Conference on High Energy Physics, London, 1974*, edited by J. R. Smith (Rutherford Laboratory, Chilton, Didcot, Berkshire, England, 1974).

[2]CERN-Hamburg-Orsay-Vienna ISR Collaboration: E. Nagy *et al.*, CERN report submitted to the XVII International Conference on High Energy Physics, London, 1974 (unpublished) [$pp \to p(n\pi^+)$ at $\sqrt{s} = 23$ to 62 GeV].

[3]Northwestern-Rochester-Fermilab Collaboration, J. Biel *et al.*, reports submitted to the International Conference on High Energy Physics, Palermo, 1975 (unpublished) ($np \to pp\pi^-$ from 50 to 300 GeV/c).

[4]Aachen-UCLA-UC Riverside-CERN ISR Collaboration: R. Webb *et al.*, Phys. Lett. B55, 331 (1975); B55, 336 (1975) [$pp \to p(p\pi^+\pi^-)$ at $\sqrt{s} = 45$ GeV].

[5]U. Amaldi, Rapporteur's report, in proceedings of the Second International Conference on Elementary Particles, Aix-en-Provence, 1973 [J. Phys. (Paris) Suppl. 34, C1-241 (1973)].

[6]N. Sakai and J. N. J. White, Nucl. Phys. B59, 511 (1973); Nuovo Cimento Lett. 8, 618 (1973); M. Jacob and R. Stroynowski, Nucl. Phys. B82, 189 (1974); G. Kane, Acta. Phys. Pol. B3, 845 (1972).

[7]R. M. Edelstein *et al.*, Phys. Rev. D5, 1073 (1972); J. V. Beaupre *et al.*, Nucl. Phys. B66, 93 (1973); J. Hanlon *et al.*, Phys. Rev. D 12, 673 (1975); Scandinavian Bubble Chamber Collaboration, unpublished data on $pp \to pn\pi^+$ at 19 GeV/c, as quoted by G. Kane, Ref. 6.

[8]For a review and list of references to earlier work, consult E. L. Berger, Argonne Report No. ANL-HEP 7506, Daresbury Study Weekend Series No. 8, edited by J. B. Dainton and A. J. G. Hey; E. L. Berger, Phys. Rev. 166, 1525 (1968); 179, 1567 (1969).

[9]H. Miettinen and P. Pirilä, Phys. Lett. 40B, 127 (1972).

[10]J. D. Jackson, Rev. Mod. Phys. 42, 12 (1970); F. S. Henyey, G. L. Kane, J. Pumplin, and M. Ross, Phys. Rev. 182, 1579 (1969).

[11]M. L. Good and W. D. Walker, Phys. Rev. 120, 1857 (1960); E. L. Feinberg and I. Pomeranchuk, Nuovo Ci-

mento Suppl. 3, 652 (1956); A. Białas, W. Czyż, and A. Kotański, Ann. Phys. (N.Y.) 73, 439 (1972); J. Pumplin, Phys. Rev. D 4, 3482 (1971); 7, 795 (1973).
[12]V. A. Tsarev, Phys. Rev. D 11, 1864 (1975). See also G. Cohen-Tannoudji and U. Maor, Phys. Lett. B57, 253 (1975).
[13]S. Humble, Nucl. Phys. B76, 137 (1974); B86, 285 (1975).
[14]G. C. Fox, in *Experimental Meson Spectroscopy—1972*, proceedings of the Third International Conference on Experimental Meson Spectroscopy, Philadelphia, 1972, edited by Kwan-Wu Lai and Arthur H. Rosenfeld (A. I. P., New York, 1972).
[15]G. Ascoli *et al.*, Phys. Rev. D 8, 3894 (1973); 9, 1963 (1974).
[16]E. L. Berger and A. Irving, this issue, Phys. Rev. D 12, 3444 (1975).
[17]E. L. Berger, Phys. Rev. D 11, 3214 (1975).
[18]See, e.g., E. L. Berger and G. C. Fox, Phys. Rev. 188, 2120 (1969).
[19]Yu. M. Antipov, *et al.*, Nucl Phys. B63, 153 (1973). We are grateful to R. Cutler for calling our attention to Table 1 of this reference.
[20]E. L. Berger, Phys. Rev. Lett. 21, 701 (1968).
[21]Yu. M. Antipov *et al.*, Nucl. Phys. B86, 381 (1975).
[22]E. L. Berger and G. C. Fox, in *Proceedings of the Second International Conference on Polarized Targets*. edited by G. Shapiro (Univ. of Calif. Press, Berkeley, Calif., 1971); G. C. Fox, Phys. Rev. D 9, 3196 (1974).
[23]CERN-Orsay-Oxford Collaboration: L. Dick *et al.*, Phys. Lett. B57, 93 (1975).
[24]G. Brandenburg *et al.*, Nucl. Phys. B45, 397 (1972).